PhD in Chemical Science
XXV Cycle (2009-2012)

University of Catania

A Low Temperature Post Production Treathment of Organic Thin Films for Photovoltaic Applications based on the application of an External Electric Field

Anna Pietrzak

Tutor: Prof. G. Marletta
Coordinatore: Prof. G.Musumarra

An undertaking such as this can never be accomplished in isolation; it is only through the support and advice of many others, both technical and moral, that it can be carried out.

I would like to acknowledge the LAMSUM research group of the Department of Chemical Science of the University of Catania and the London Centre for Nanotechnology team of the College University of London. Their collective technical guidance added much to the content of this work.

In particular I would like to mention Professor Giovanni Marletta, my thesis advisor, and Professor Franco Cacialli, my supervisor during the time I spent at the University College as a visiting researcher, for their continuous support and significant advices.

Lastly, but by no means lesser in importance, I would like to thank my family and friends for their moral support during the time of this effort. While technical advice is necessary, it is by no means sufficient. Without their encouragement, none of this work would have been possible.

Table of contents

List of figures

List of tables

Abbreviations

AFM	Atomic Force Microscope
AM1.5	
BHJ	Bulk Heterojunction
CP	Conjugated polymer
e-	Electron
E.Q.E	External Quantum Efficiencies
Ea	Electron affinity
Ef	Fermi level
Eg	Bandgap
eV	Electron Volt
FF	Fill factor
η	Overall solar cell efficiency
HBTP	5,7-Bis-(5'-hexyl-[2,2']bithiophenyl-5-yl)-2,3-dimethyl-thieno[3,4-b]pyrazine
HOMO	Highest Occupied Molecular Orbital
IP	Ionisation potential
Jsc	Short circuit current
ITO	Indium tin oxide
λ	Wavelength
LUMO	Lowest Unoccupied Molecular Orbital
mA	mili Amper
min	minutes
nm	nanometre
OLED	Organic Light Emitting Diode
OPV	Organic Photovoltaics
OSCs	Organic Solar Cells
P3HT	Polythiophene
PCBM	[6,6]-phenyl-C_{61}-butyric acid methyl ester
PCE	Power conversion Efficiency

PEDOT:PSS	poly(ethylene dioxythiophene), doped with polystyrene sulphonic acid
PL	Photoluminescence
PPV	Poly-phenylenevinylene
rpm	round per minute
RR	Regioregular
s	seconds
Voc	Open-circuit voltage

1 Introduction

1.1 World energy demand and green house gas emissions

Fossil fuels have been at the basis of the economy of industrialized countries during the twentieth century. The standard of living of these countries could not have developed without hydrocarbons like coal, oil, and natural gas. Beside the use in satisfying the request of energy, a variety of products exist which are based on this type of natural resources. More recently, developing countries in the far east and South America have also contributed in the increase of the demand of hydrocarbons, and, in particular those used to satisfy the world energy demand. However, these achievements come with a price. Global warming is overwhelming; and there is evidence for anthropogenic causes related to the combustion of fossil fuels [1].

The average atmospheric CO_2 concentration in 2009 was 387 ppm [4]. In 2007, the Intergovernmental Panel on Climate Change produced

an extensive report outlining what are the thresholds within which green house gases (GHGs) should be contained; and beyond which drastic climatic change would likely be inevitable [2]. It was reported that in order to maintain the atmospheric carbon dioxide concentration below 450 ppm, carbon dioxide emissions should be reduced by 80%[1] by 2050. According to some scientists a safe threshold should be defined at 350 ppm; which was already passed in 2009 [3].

The United States currently consumes approximately one fourth of the energy consumed by the entire world. The combustion of fossil fuels in 2009 supplied 83% of this energy; while renewable only 8% of the total [2]. A return to a pre-industrial era is impossible. Renewable energy (wind, solar, hydroelectric, geothermal, or nuclear) will have to supply a significant portion of our power in the near future (Figure 1.1.1).

Figure 1.1.1. Two different vision of the future on earth. Thanks to renewable energy like wind, solar, hydroelectric, geothermal, we can avoid the hypothesis pictured on the left.

[1] 80% below 1990 levels

1.2 Solar energy and solar cell devices

The sun provides us daily with large quantities of energy, which is enough to meet much more of the current levels of global energy demand. In only one hour it supplies more energy that the world need in one year. It is not surprising that the prospect of converting the solar light into electricity is highly tempting and several applications of different sizes have already been realized. However, according to the RENI21[2], in 2010, the energy produced by photovoltaic conversion accounted for only the 0.06% of the total consumption.

Solar cell devices are generally layered structures with a light absorbing and semiconducting active layer or material sandwiched between two electrodes. The band gap (i.e., the energy gap between the valence band and the conduction band)[3] of solar cells is such that their electrical conductivity is somewhere between that of a metal and that of an insulator, see Figure 1.2.1 [5].

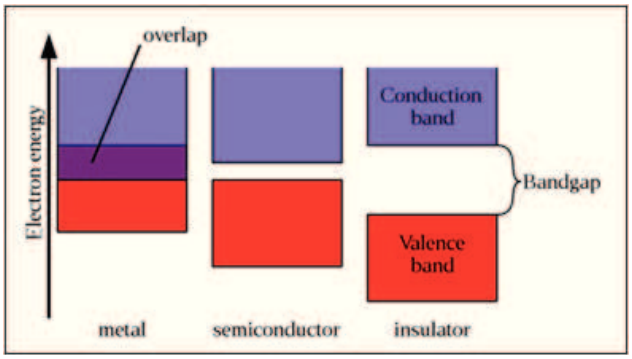

Figure 1.2.1. A simplified diagram illustration the energy band levels of an insulator, a semiconductor, and a conductor. Electrons can only exist in certain energy levels.

[2]RENI21, Global Status Report, 2012

The size of the band gap highly influences the conductivity of a material [6]. Semiconductors have an intermediate band gap (tipicaly 0.5 to 3 eV). When semiconductors are exposed to light, the small band gap allows to harvest the energy absorbed from photons, i.e., excited electrons jump from the valence band to the conduction band; creating electron-hole pairs, the so-called excitons. Successively, exciton dissociation allows the separation of charges (the electrons and holes) that are transported to the electrodes and eventually produce a current in an external circuit [5, 7].

Several different concepts and materials are used for making solar cells. In p-n homojunction a semiconductor that has two doped regions, one with excess of holes (p-type) and another with excess of electrons (n-type), is used as the active material [5]. The excess charge carriers will diffuse over the junction between the doped regions; giving as result a net positive and negative charge on each side of the junction [7]. Thus, an internal electrostatic field, sufficient to separate the photo-generated electrons and holes, is induced in the cell (see Figure 1.2.2).

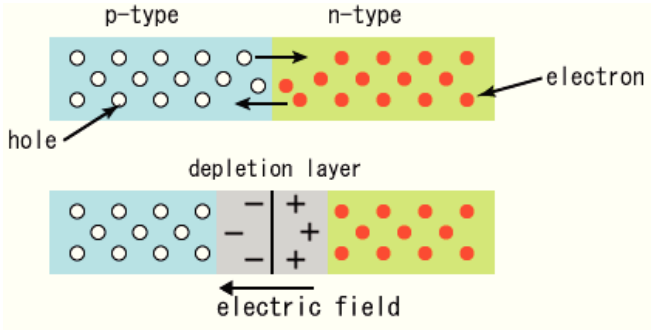

Figure 1.2.2. A schematic image of p-n junction solar cell. When the incident light is absorbed, electron- hole pairs are generated which are separated by the electric field in the space charge region, resulting in a photocurrent that can be extract in an external circuit.

Silicon based solar cells dominate the solar cell market but other inorganic semiconductors (e.g., gallium arsenide, cadmium telluride) are also used as the active material [8]. The voltage and the current generated by a single solar cell are about 0.5 to 1 V and some tens of mA/cm2, respectively [5]. Series connections help are used to increase the device voltage, which is too low for most applications. Finally, a *module* is a panel of encapsulated and connected solar cells. Current levels of power conversion efficiency[4], for standard silicon based solar modules are about 15 % [8], which is higher for single solar cells, due to losses generated mainly at the connections in the module. Quality of silicon also influence strongly the performance of silicon solar cells (i.e., monocrystalline and polycrystalline). One the limiting factors of the diffusion of this kind of cells is the price w.r.t. fossil fuels. Currently, the for the electricity generated from solar cells is about 7 and 24 €cent/kWh [9]. One reason lays in the high costs involved in the production of crystalline silicon cells e.g. crystal growth.

Developments in the production of solar cells have rendered the production more effective. Other materials than silicon have been used and other production techniques have been developed (e.g., chemical vapour deposition of silicon and copper indium gallium diselenide [10, 11]). New kind of solar cells are dye-sensitized solar cell and solar cells based on organic materials. The dye-sensitized solar cell, also known as the Grätzel cell, is a photoelectrochemical cell based on a semiconductor and an electrolyte [12]. One of their main advantage is that they can be produced on flexible substrates and fabricated in series manufacturing processes (e.g., ink-jet).

---

[3]Crystalline solids have a delocalized electronic structure that forms allowed and forbidden energy bands. The band gap is the energy gap between the top of the highest allowed band (filled with electrons) and the bottom of the lowest allowed band (empty of electrons)

Another type of solar cells is based on organic materials. In this cells excitons are more strongly bound and more localised than in crystalline solids [15]. Generally, a combination of two materials with different electron affinities is used (i.e., a donor and an acceptor) in order to favor the separation of electrons and holes at the interface between the two materials. Thus, a charge transfer occurs, where the donor material donates an electron to the acceptor material. The best power conversion efficiencies reported for organic and polymer based solar cells are so far relatively low, around 5% [15-19]. Current efforts for improving the performance of organic solar cells are based on: (i) the study of the underlying physical processes of photocurrent generation, charge separation and transport; (ii) on the synthesizing of new polymers; (iii) the improve of the device structure and the manufacturing process [20].

Whilst organic photovoltaic cells (OPVs) have not yet reached the technological maturity sufficient for their widespread commercialisation (i.e. by combining high efficiency, long lifetime and low cost), rapid growth in the research and development of OPVs has occurred over the past decade. In the literature, the published record PCE now stands at over 8% and OPVs with lifetimes approaching seven years have also been demonstrated.

1.3 Contribution of this thesis

The purpose of this thesis is to develop our understanding of the mechanisms of film structure formation and modification of a PV applicable organic thin film; and to understand how this impacts upon the photovoltaic efficiency of an OPV device.

---

[4] The ratio of output electrical power to incident optical power

To achieve this goal, after an introduction of conjugated materials and device structure and preparation is given in Chapter 2 and 3, respectively, Chapter 4 reports of experiments performed on P3HT and PCBM bulk heterojunction solar cells where different preparation conditions were applied. Both electrical and morphological analyses were carried out highlighting the main relations between the preparation parameters and the electrical properties of devices.

In Chapter 5 we report on an investigation made on the effect of post-treatment production processes such as thermal annealing and external electric field application. This chapter focuses in finding an alternative to high temperature treatments for low-cost low-temperature fabrication of solar cell devices and finds a possibility in the use of an external electric field in absence of any post-thermal treatment.

Beside the study of the factors driving the efficiency of OPVs, stability over time is a major issue, too often not properly considered, if not at all. Organic solar cells are complicated multilayer structures where each component may fail for different reasons and layers may even interact chemically and physically in ways that may cause degradation. Chapter 6 discusses the issue of degradation and compares two different implementations: encapsulated *vs* non-encapsulated devices.

Finally, controlling the morphology of the device is only a part of the path to high-efficient OPVs. The choice of the material influences both electrical properties and the processes for the correct controlling of the morphology of the active layer of devices. Chapter 7 completes this thesis with the characterization (in photovoltaic terms) of a new small-molecule donor system, HBTP, for use in organic plastic solar cells, with electron acceptor molecule PCBM.

References

[1] N. Oreskes. *Science*, **2004**, *306*, 1686.

[2] IPCC 4th Report, **2007**. http://www.ipcc.ch

[3] B. McKibben. The tipping point. Yale Environment 360, June 3 2008.

[4] National Oceanic US Department of Commerce and Atmospheric Administration. Trends in carbon dioxide. Earth System Research Laboratory, **2010.**

[5] J. Nelson, in *The Physics of Solar Cells*, Imperial College Press, London, **2003**.

[6] N.W. Ashcroft, N.D. Mermin, in *Solid State Physics*, Thompson Learning, Inc., London, **1976**.

[7] D.A. Neamen, in *Semiconductor Physics and Devices: Basic Principles*, McGraw-Hill, New York, **2003**.

[8] "*Solceller - Teknik, marknad och svensk forskning 2000-2005,*" **2006**.

[9] "*Solar Generation IV - 2007. Solar electricity for over one billion people and two million jobs by 2020.,*" **2007**.

[10] A. Goetzberger et al, *Mater. Sci. Eng., R* **2003,** *R40*, 1.

[11] R.N. Bhattacharya et al, *Appl. Phys. Lett.* **2006,** *89*, 253503.

[12] M. Gratzel, *Nature* **2001,** *414*, 338.

[13] A. Hagfeldt, M. Gratzel, *Acc. Chem. Res.* **2000,** *33*, 269.

[14] M. Quintana et al, *J. Phys. Chem. C* **2007,** *111*, 1035.

[15] J.J.M. Halls et al, *Phys. Rev. B: Condens. Matter* **1999,** *60*, 5721.

[16] J. Peet et al, *Nat. Mater.* **2007,** *6*, 497.

[17] M. Reyes-Reyes et al, *Appl. Phys. Lett.* **2005,** *87*, 083506.

[18] W. Ma et al, *Adv. Funct. Mater.* **2005,** *15*, 1617.

[19] G. Li et al, *Nat. Mater.* **2005,** *4*, 864.

[20] J. Nelson, *Curr. Op. Sol. State Mater. Sci.* **2002,** *6*, 87.

2 Conjugated materials

2.1 Electronic structure

Electronic conductivity in *polyacetylene* was discovered in 1977 (see Figure 2.1.1) [1]. This signed the beginning of the study of conjugated polymers in several engineering applications. The discovery was awarded with the Nobel prize in Chemistry 2000 [2].

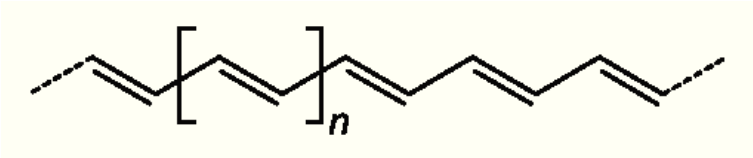

Figure 2.1.1. Polyacetylene.

Polyacetylene is the simplest conjugated polymer. The chain consist only of single and double carbon-carbon alternating bonds. In polymers with alternating single and double bonds between the carbon atoms in the backbone, each carbon only bonds to the three nearest neighbors. Carbon atoms are in a sp^2 hybridized state forming three covalent σ-bonds and leaving one electron in an unhybridized pz orbital [3]. The carbon atoms are said to be unsaturated. The unhybridized pz orbitals of each carbon atom lie perpendicular to the plane of the sp^2 hybrid orbitals, resulting in an *overlap* of the pz orbitals and the formation of a *π-bond*. In polymers with this configuration, i.e. with alternating single and double bonds in the polymer backbone, the π-states are *delocalised* along the polymer chain [4,5]. Such polymers are known as *conjugated polymers*.

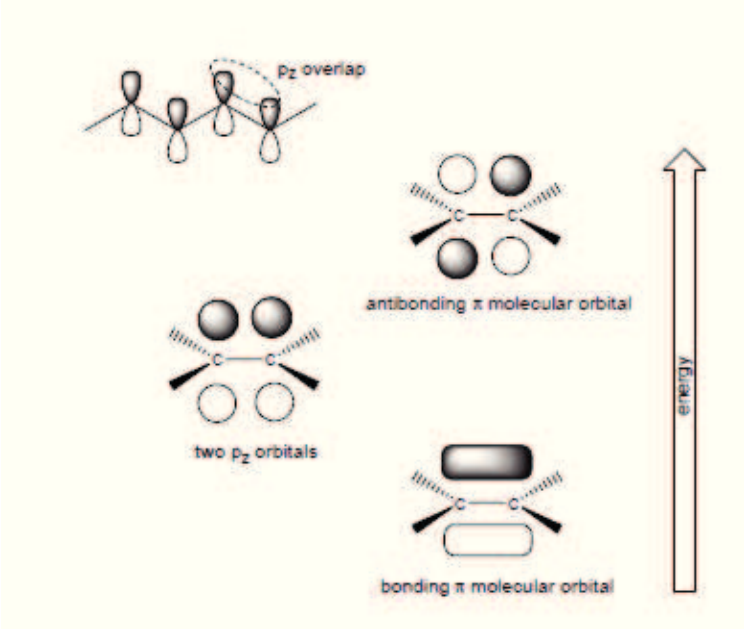

Figure 2.1.2 Two different molecular π-orbitals - bonding and antibonding

Two pz orbtials combine to form molecular π-orbitals, one bonding with lower energy and one antibonding with higher energy (see Figure 2.1.2) [3]. The bonding π-orbital, being the lower energy orbital, contains both the π-electrons while the antibonding π*-orbital is unoccupied. The energy gap between the highest occupied molecular orbital (HOMO) and the lowest unoccupied molecular orbital (LUMO) for conjugated polymers is in the range of 1 – 4 eV [4].

The electron affinity of a polymer corresponds to the energy of the LUMO (w.r.t. the vacuum level) and the ionization potential corresponds to the energy of the HOMO. In inorganic solids LUMO and HOMO energy levels are considered as corresponding to the lowest state of the conduction band and the upper state of the valence band, respectively. However, since most polymers are amorphous disordered materials with week interchain interactions, they present defects and kinks in the chain which may act as energy barriers for electrons, i.e., disorder limits the delocalization (conjugation) length of the π-electrons along the polymer chain [6, 7]. As a consequence of week interchain interactions, charge transport between polymer chains is strongly dependent on the degree of interchain overlap and chain packing. Moreover, electron-hole pairs (i.e., excitons) in conjugated polymers are: (i) more strongly bound by Coulomb interaction; (ii) and more localized; than in crystalline solids [4, 5, 7, 8].

2.2 Materials

Properties of polymers can be chemically manipulated with a variety of easy and cheap processing techniques. This fact has made polymer-based materials present in almost every aspect of modern society.

Conjugated polymers with band gaps in the same range (1-4 eV) of inorganic semiconductors can be used to fabricate transistors and diodes.

Nowadays, the efficiency of polymeric solar cells are around 10% [9], much lower compared to crystalline silicon solar cells but in the past decades improvements have been made to consider this technology promising.

Advantages of using conjugated polymers compared to inorganic semiconductors lies:

- in their difference in mechanical properties (where polymer solar cells can be produced on flexible or bendable substrates [10,11]);
- in processing advantages (where polymers can generally be processed from solution which opens for the use of less expensive production techniques).

Usually, polymers are divided into groups based on their repeating unit (monomer) in the backbone. Varying the physical and mechanical properties of the polymers can be done by adding different *side-chains* (solubility improvement), or by incorporating another repeating unit in the backbone (e.g., *co-polymerization*). In particular, these techniques may change the size and position of the band gap of the polymer [12,13]. Figure 2.2.1. show some common conjugated polymers used in solar cell applications.

Disadvantages of conjugated polymers are: (i) photo-oxidation; (ii) instability in the presence of oxygen or water, especially in combination with light; and (iii) survivability (to reach long lifetimes the devices have to be encapsulated (more in chapter 6).

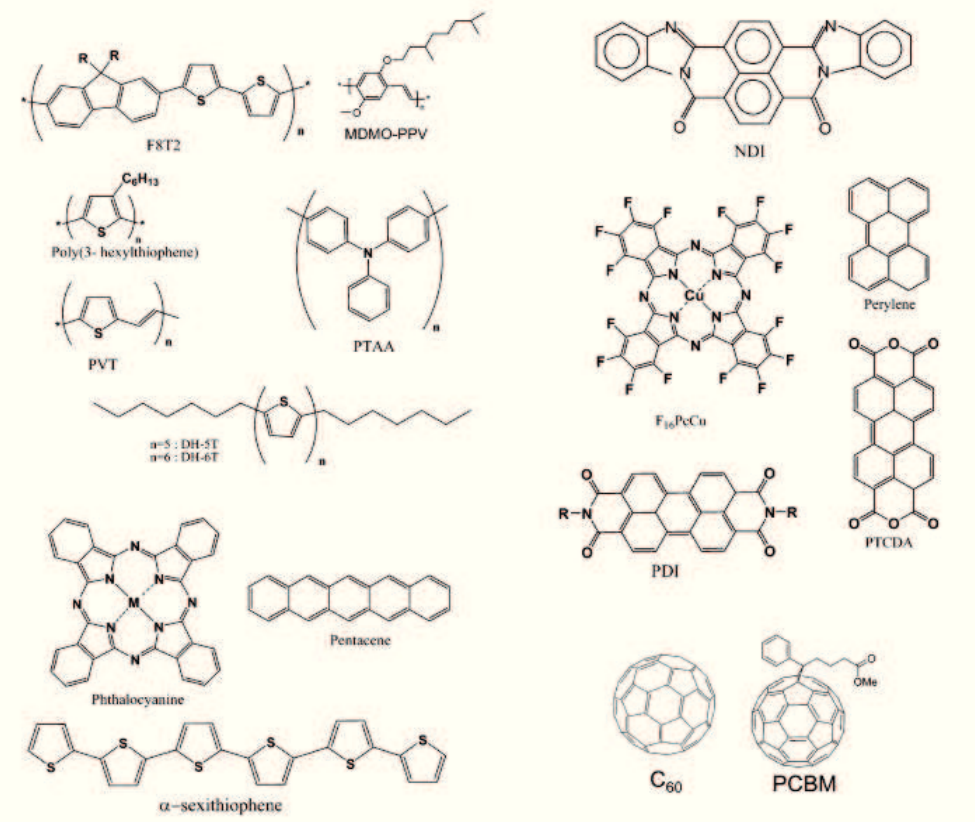

Figure 2.2.1. Chemical structures of some conjugated polymers used in solar cell applications [13].

2.3 Donors and acceptors

In conjugated polymers excitons are strongly bound by Coulomb interactions, compared to in inorganic semiconductors. In solar cell

applications, this results in poor generation of free charges when a single polymer is used in the active layer. This problem has been solved by using a combination of two materials with a difference in *electron affinity*. The difference can be used to obtain a charge transfer between the two materials, where one material (the donor) donates an electron and the other material (the acceptor) accepts one electron [14].

The requirement for charge transfer between donor and acceptor is that the LUMO of the donor material should be located sufficiently (~0.5 eV) above the LUMO of the acceptor, and that the HOMO level of the acceptor should be below the HOMO of the donor [14]. A number of different combinations of donor and acceptor polymers have been used in solar cells [15-18].

It is also possible to combine conjugated polymers with other molecular materials or inorganic nanoparticles (e.g., see [19] for applications with fullerene C_{60}. The most common fullerene derivative, used in polymer solar cells, is [6,6]-phenyl-C_{61}-butyric acid methyl ester (PCBM) [20,21] (Figure 2.3.1).

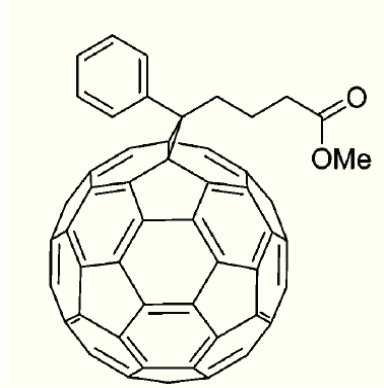

Figure 2.3.1. Chemical structure of PCBM.

Also other small molecules have been used as acceptor materials in polymeric solar cells, see for instance [22-30].

2.4 Transport properties

Electron and hole mobilities are an important factor in the choice of donor and acceptor materials for solar cell applications. For efficient transport of the charges to the electrodes, the donor should be an efficient electron conductor and the acceptor should have good hole transport properties.

Most conjugated polymers used in solar cells are amorphous and have poor charge carrier mobilities in the range of 10^{-3} to 10^{-5} cm^2/Vs [29]. In P3HT, which has a crystalline phase, an ordering of the polymer chains (i.e. crystallization) has been reported to increase the mobility by up to two orders of magnitude, reaching mobilities in the range of 10^{-2} cm^2/Vs [30]. One of the main reasons for the popularity and frequent use of PCBM as the acceptor material in polymer solar cells is that it is a *good electron conductor*, with an electron mobility around 10^{-2} cm^2/Vs [31,32].

2.5 Absorption

The standardized AM1.5 (air mass 1.5) solar irradiance spectrum as a function of wavelength for solar cell measurements can be seen in Figure 2.5.1. The spectrum corresponds to an angle of incidence of solar radiation of 48° relative to the surface normal for a set of specified atmospheric conditions [33,34].

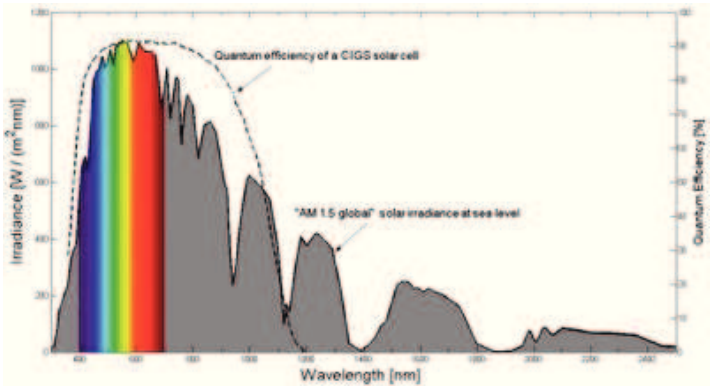

Figure 2.5.1. Standardized AM1.5 solar spectrum.[27]

Irradiance, i.e. the amount of radiant energy per unit area and unit time, is larger in the visible region (300-800 nm) with a peak in the blue-green [35].

Many conjugated polymers absorb from the ultraviolet to the blue wavelength (500 nm) region [36], but the solar photon flux density (the number of photons with energy in the range E, E+dE incident on a unit area in a unit time), has its maximum around 700 nm [33]. The irradiance L(E) and the photon flux density b(E) are related according to the equation (2.5.1) [35]:

$$L(E) = E \cdot b(E). \tag{2.5.1}$$

Since, ideally, each incident photon will generate one exciton and eventually one electron in the external circuit, a good overlap with the solar photon flux density is required for generating as many excitions as possible and extracting large currents from solar cells.

In recent years efforts have been put into synthesising intermediate and low band gap (<1.8 eV) conjugated polymers [37,42] to

improve the absorption at longer wavelengths, e.g., incorporating segments consisting of alternating electron-donating and electron-accepting units (D-A-D segment) in the polymer repeating unit [38,43]. Polymer solar cells with absorption extending as far as in to the infrared region has been achieved with this strategy [44].

From this point of view, PCBM has a drawback in that it only absorbs light with wavelengths shorter than 470 nm [44] and thus contributes very little to the absorption of solar light.

Beside exploring new acceptor materials, another way to improve the overall absorption of solar light is to stack solar cells based on materials that absorb in different wavelength regions (e.g., tandem cells) [45-47].

References

[1] C.K. Chiang et al, *Phys. Rev. Lett.* **1977,** *39*, 1098.

[2] http://nobelprize.org/chemistry/laureates/2000/chemadv.pdf, The Nobel Foundation, **2007**.

[3] T.W.G. Solomons, in *Organic Chemistry*, John Wiley & Sons, Inc., New York, **1996**.

[4] W.R. Salaneck et al, *Physics Reports* **1999,** *319*, 231.

[5] A.J. Heeger, *Rev. Mod. Phys.* **2001,** *73*, 681.

[6] J.M.G. Cowie, in *Polymers: Chemistry & Physics of modern materials*, Stanley Thornes, Cheltenham, **1991**.

[7] B.J. Schwartz, *Annu. Rev. Phys. Chem.* **2003,** *54*, 141.

[8] J.J.M. Halls et al, *Phys. Rev. B: Condens. Matter* **1999,** *60*, 5721.

[9] http://www.heliateck.com

[10] C.J. Brabec et al, *Adv. Funct. Mater.* **2001,** *11*, 15.

[11] C. Lungenschmied et al, *Sol. En. Mater. Sol. Cells* **2007,** *91*, 379.

[12] M.R. Andersson et al, *Macromolecules* **1995,** *28*, 7525.

[13] A.C. Grimsdale et al, *Synth. Met.* **1996,** *76*, 165.

[14] J.J.M. Halls et al, *Phys. Rev. B: Condens. Matter* **1999,** *60*, 5721

[15] J.J. Halls, R.H. Friend, in *United States Patent*; Cambridge Display Technology Limited, Cambridge, **2003**, 67.

[16] J.J.M. Halls et al, *Adv. Mater.* **2000**, *12*, 498.

[17] M.M. Koetse et al, *Appl. Phys. Lett.* **2006**, *88*, 083504.

[18] S.C. Veenstra et al, *Chem. Mater.* **2004**, *16*, 2503.

[19] N.S. Sariciftci et al, *Science* **1992**, *258*, 1474.

[20] C.J. Brabec, *Sol. En. Mater. Sol. Cells,* **2004**, *83*, 273.

[21] P.W.M. Blom et al, *Adv. Mater.* **2007**, *19*, 1551.

[22] S.A. Jenekhe, S. Yi, *Adv. Mater.* **2000**, *12*, 1274.

[23] J.J. Dittmer et al, *Sol. En. Mater. Sol. Cells.* **2000**, *61*, 53.

[24] W.U. Huynh et al, *Phys. Rev. B: Condens. Matter.* **2003,** *67*, 115326.

[25] B. Sun et al, *J. Appl. Phys.* **2005**, *97*, 014914.

[26] W.J.E. Beek et al, *J. Phys. Chem. B* **2005**, *109*, 9505.

[27] J.A. Rud et al, in *J. Mater. Sci.* Badajoz, Spain, **2005**, 03, 1455.

[28] B.J. Landi et al, *Prog. Photovoltaics: Research and Applications* **2005,** *13*, 165.

[29] M. Redecker et al, *Adv. Mater.* **1999,** *11*, 241.

[30] Z. Bao et al, *Appl. Phys. Lett.* **1996,** *69*, 4108.

[31] T.D. Anthopoulos et al, *Adv. Mater.* **2004,** *16*, 2174.

[32] S.M. Tuladhar et al, *Adv. Funct. Mater.* **2005,** *15*, 1171.

[33] P. Würfel, in *Physics of Solar Cells - From Principles to New Concepts*, Wiley-VCH, Weinheim, **2005**.

[34] http://rredc.nrel.gov/solar/spectra/am1.5/, National Renewable Energy Laboratory - Reneable Resource Data Center, **2007**, 68.

[35] J. Nelson, in *The Physics of Solar Cells*, Imperial College Press, London, **2003**.

[36] C.J. Brabec et al, *Adv. Funct. Mater.* **2001,** *11*, 15.

[37] J. Peet et al, *Nat. Mater.* **2007,** *6*, 497.

[38] E. Perzon et al, *Polymer* **2006,** *47*, 4261.

[39] W. Mammo et al, *Sol. En. Mater. Sol. Cells* **2007,** *91*, 1010.

[40] A. Dhanabalan et al, *Adv. Funct. Mater.* **2001,** *11*, 255.

[41] M.M. Wienk et al, *Appl. Phys. Lett.* **2006,** *88*, 153511.

[42] S.W. Suk et al, *J. Polym. Sci., Part A: Polym. Chem.* **2007,** *45*, 1394.

[43] C. Kitamura et al, *Chem. Mater.* **1996,** *8*, 570 L2.

[44] X. Wang et al, *Appl. Phys. Lett.* **2004,** *85*, 5081.

[45] J. Gilot et al, *Appl. Phys. Lett.* **2007,** *90*, 143512.

[46] G. Dennler et al, *Appl. Phys. Lett.* **2006,** *89*, 073502.

[47] A. Colsmann et al, *Appl. Phys. Lett.* **2006,** *89*, 203506.

3 Device Characterization

3.1 Current-voltage characteristics

The performance of a photovoltaic device can be evaluated through the *current-voltage characteristic* of the device in the dark and under illumination. Figure 3.1.1 shows a typical current-voltage characteristic. The analysis of this curve gives a set of information: the short-circuit current; the open-circuit voltage; the fill factor; and the power conversion efficiency, of the device.

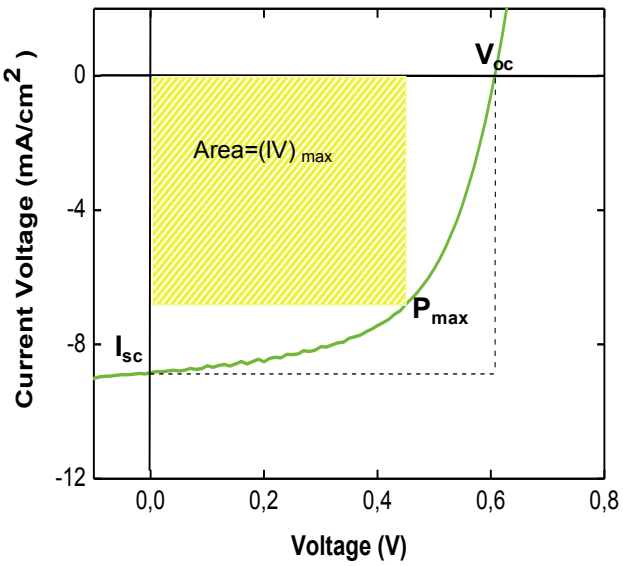

Figure 3.1.1. Current-voltage characteristics for a solar cell under illumination.

A solar cell produces a photocurrent when illuminated. The photocurrent at exactly zero bias is called the *short-circuit current* (I_{sc}). However, the common used quantity is the *short-circuit current density* (J_{sc}), which is the current divided by the active diode area.

If a forward bias is applied, the resulting current (said "dark current") and the photocurrent move on opposite verse. Therefore, the overall current in the device is the short-circuit current reduced by the opposing dark current[1] as described in the following relation [1]:

$$J(V) = J_{sc} - J_{dark}(V). \tag{3.1}$$

[1] under illumination and at an applied forward bias V

The voltage at which the net current is zero is known as the *open-circuit voltage*, (V_{oc}). It defines the operating range of solar cells (from 0 bias to V_{oc}). The power generated by the device is given by the relation:

$$P = I \cdot V. \tag{3.2}$$

We denote with V_{mpp} and I_{mpp} the voltage and the current, respectively, where the power generated from the device has its maximum, called P_{max}. From these quantities, *the fill factor* (FF) of the device is retrieved as [2]:

$$FF = \frac{V_{mpp} \cdot I_{mpp}}{I_{sc} \cdot V_{oc}}. \tag{3.3}$$

FF describes the shape of the current-voltage. The more rectangular the shape of the curve the greater the FF.

Finally, the *power conversion efficiency*, η, is obtained as:

$$\eta = \frac{P_{max}}{P_L}, \tag{3.4}$$

where P_L is the power of the incident light.

Sandardized measurement conditions are used around the world to compare the parameters of different solar cells. The standard reporting conditions are: illumination by white light at an intensity of 1000 W/m2 with a AM1.5 global spectrum and a sample temperature of 25 °C [2] (see Chapter 3.8).

3.2 Quantum efficiency

Another important quantity for describing the performance of a solar cell is the *external quantum efficiency* (EQE), known also as the *incident photon to current efficiency* (IPCE). The quantity is obtained dividing the short-circuit current evaluated at each wavelength of the spectral response[2] of a device by the intensity of that light. The resulting spectrum gives information about the probability of an incident photon of a specific wavelength generating an electron to the external circuit [1].

EQE depends on the *absorption coefficient* of the active layer but also on the *efficiency of the charge separation*, *transport* and *collection*. Correcting the EQE spectra for optical losses due to the transmission and the reflection of light of the solar cell an internal measure, the so-called *internal quantum efficiency*, can be obtained [3]. Since this quantity depends only on charge generation and transport properties, is useful in comparative analyses of devices.

3.3 Donor-acceptor polymeric solar cells

As a solar cell is composed of a donor and an acceptor. The choice of electrodes is influenced by their molecular structure. In particular (Figure 3.3.1) [4]:

- the work-function of the anode (φanode) should be smaller or equal to the ionization potential of the donor (HOMO level);
- the work-function of the cathode (φcathode) should be larger or equal to the electron affinity of the acceptor (LUMO level).

V_{oc} correlates directly to the energy difference between the HOMO of the donor and the LUMO of the acceptor [5] (ohmic contrast, where in a non-homic). On the other hand, for non-ohmic contrast V_{oc} scales with the work-function difference of electrodes.

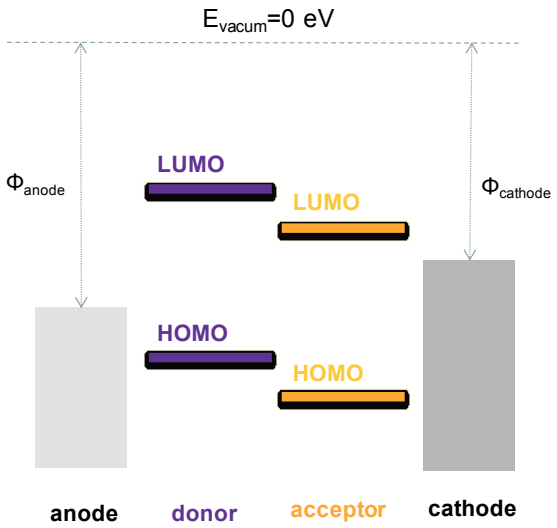

Figure 3.3.1. The energy levels of the donor, acceptor and electrode materials (correlated to the E_{vaccum}).

The processes that conduces to the generation of the photocurrent can be summarized as follow (see Figure 3.3.2):

1. absorption of the light and generation of an exciton;

2. dissociation of the exciton and separation of the charges;

3. transport of the charges to the electrodes and collection of the charges.

Absorption can occur in any of the two donor and acceptor materials and depends on the *device geometry;* the *absorption coefficient* and the *thickness* of the donor-acceptor layer. The absorption spectra of the materials should overlap with the solar spectrum of the photon flux density to generate as many excitons as possible.

Excitons may either *recombine* resulting in an emission of light (photoluminescence) or *dissociate at an interface* between the donor and acceptor materials. In the second case a *charge transfer* from the donor to the acceptor or from the acceptor to the donor takes place.

Separated charges are then transported to the electrodes. At short-circuit current (as in Figure 3.3.2) the direction of the current is determined by the work-function of the electrodes.

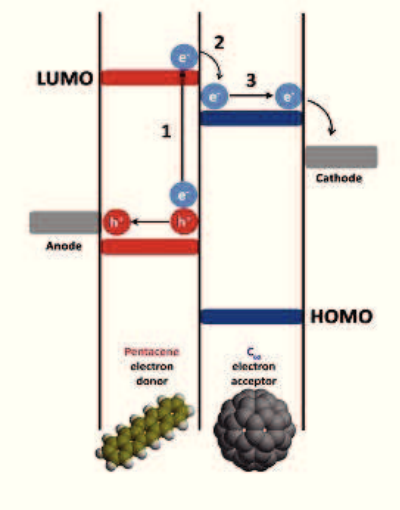

Figure 3.3.2. The physical processes in a solar cell (at short-circuit current condition) divided into three steps: (1) absorption of a photon (hν) in the donor and generation of an exciton, (2) dissociation of the exciton and charge transfer of an electron to the acceptor, (3) transport and collection of the charges.

High power conversion efficiencies for solar cells are obtained depending on the values of V_{oc}, J_{sc} and FF. The following arguments can be made:

- V_{oc} is determined by the solar cell material and the electrodes.

- A high fill factor depends on an efficient exciton dissociation and separation of the charges [6] and balanced electron and hole mobilties [7].
- To obtain a high J_{sc} both an efficient light absorption as well as efficient charge generation, transport and collection are required.

In conclusion all the 3 processes presented above are strongly influenced by the *device structure* and the distribution of the donor and the acceptor material (*morphology*) in the cell.

3.4 Basic structure of devices

Polymer solar cells consist of an active layer sandwiched between two electrodes (Figure 3.4.1).

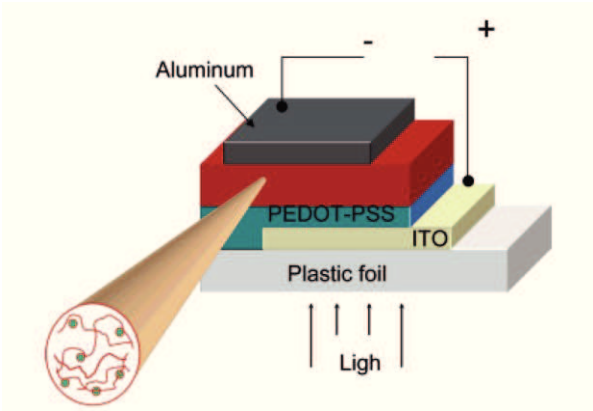

Figure 3.4.1. A schematic image (not to scale) of the layered structure of an organic solar cell and typical contact materials[8].

One electrode needs to be transparent or semi transparent to allow light to get through and currently the most suitable material is a conducting indium tin oxide (ITO) coated on a glass substrate (Figure

3.4.3). This electrode is then the hole-collecting anode. The ITO is usually covered with a thin film of PEDOT:PSS, i.e. poly(ethylene dioxythiophene), doped with polystyrene sulphonic acid (Figure 3.4.2). The layer of PEDOT:PSS smoothes the relatively rough ITO surface and helps to prevent short-circuits due to spikes in the ITO.

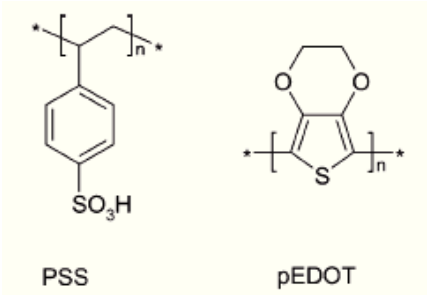

Figure 3.4.2. PEDOT:PSS poly(ethylene dioxythiophene), doped with polystyrene sulphonic acid.

Aluminium (Al) is typically used as the top electron-collecting electrode (cathode). It is evaporated through a shadow mask on top of the active layer. A thin film of LiF or Ca is sometimes introduced between the active layer and the top electrode. However, the role of this intermediate layer and how it affects the device performance is still under discussion [9-11].

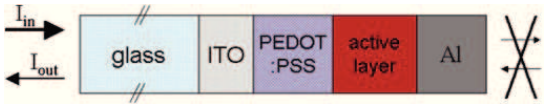

Figure 3.4.3. Schematic structure of multilayer device. The incoming light (*I*in) enters the device and propagates attenuated toward the aluminum electrode. There it is reflected, and the outgoing intensity (*I*out) leaves the device through the glass. Because of the high reflectivity of the sufficiently thick aluminum electrode, no light leaves or enters from the right side of the device [8].

Other structures have been developed, e.g. inverted [12], folded [13], semitransparent [14], tandem [15] and multijunction [16] cells.

The active layer, i.e. a thin film of the donor-acceptor materials, is usually deposited from solution using spin-coating, directly onto the bottom electrode. There are two basic structures in which the donor and acceptor materials can be combined:

- *bilayer-heterojunction*, deposition of the donor and acceptor materials in two separate layers; and
- *bulk-heterojunction,* simultaneous depositon of the two materials in one single layer.

Both the structures have their advantages and drawbacks. A general advantage for the bulk-heterojunction is that the active layer can be spin-coated from a single solution in which the donor and acceptor are dissolved in a common solvent.

3.5 Morphology

Bilayer-heterojunction structures were used in the first attempt to fabricate solar cells [17]. There are a series of techniques used to this end: spin-coating the layers on top of each other from different solvents [18], by laminating two already existing layers [19] or by evaporating C_{60} on top of a spin-coated polymer layer [20].

The main drawback of this structure is that there must be a donor/acceptor interface within the distance of 10 nm [21-25], that is, the *diffusion length of excitons*. This is due to the fact that the driving force for dissociation of the exciton and separation only exists at the interface between the two materials.

In bilayer junction solar cells (Figure 3.5.1 a) only the excitons created in such close range to the interface between the two layers succeed to dissociate.

A way to address this problem is to increase the roughness of the interface (Figure 3.5.1 b). Diffuse interface structures give more photocurrent compared to the planar bilayer devices [26-28].

Another method consists in mixing the donor and acceptor in one single layer, and achieve a bulk-heterojunction device structure (Figure 3.5.1 c) [29-31]. This method has proven to be a successful approach in several applications [32, 33].

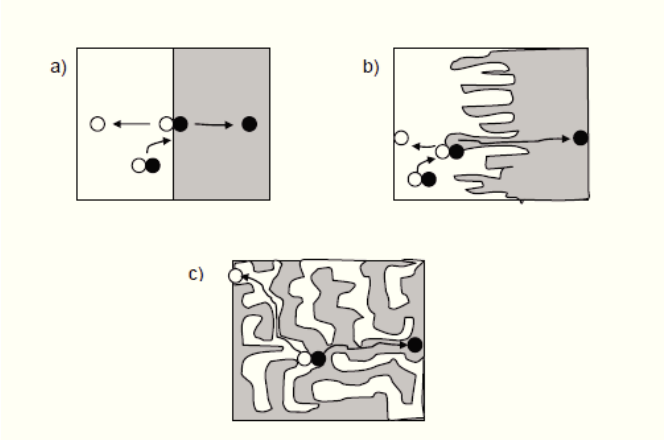

Figure 3.5.1. Schematic illustrations of different donor-acceptor active layer morphologies: a) planar bilayer-heterojunction, b) diffuse interface bilayer-heterojunction, and c) bulk-hetereojunction. Electrons and holes are indicated by closed and open circles respectively.[34]

The transport of charges to the electrodes is also affected by the morphology of the active layer. It is important that continuous paths within pure phases of each of the components are generated between the point of excition dissociation and the electrodes. This will enhance the possibility of charges generated in each material to reach the electrodes before recombining.

In bulk-heterojunction devices the existence of continuous paths depends on the 3D distribution of the two components in the layer. This kind of devices, while presenting a larger interface than bilayer devices can include both dead-ends and bottlenecks (Figure 3.5.1 c), which are responsible of trapping and recombination of charges.

This means that the performance of the bulk-heterojunction solar cells is strongly affected by the donor-acceptor blend film morphology. This is generally accepted and both solvent changes [35,36] and postproduction treatments [37] have been reported to improve the performance of bulk-heterojunction polymer solar cells. Moreover, parameters such as charge carrier mobility, which strongly influence the device performance, are intrinsic properties of each polymer/molecule. This can be illustrated by the fact that in some polymer: PCBM blends the hole mobility decrease linearly with increasing PCBM content [38] while in other blends the hole mobility increase with increasing PCBM content [39,40].

It is therefore of great importance both to understand and control the blend film morphology during spin-coating and also study the morphology together with device characterization to find the optimal morphology of a donor/acceptor combination.

3.6 Ideal structure of organic solar cells devices

The ideal structure of a bulk heterojunction solar cell is shown in Figure 3.6.1. The two phases of donor and acceptor within the bulk heterojunction have to be interspaced with an average length scale of around 10-20 nm equal to or less than the exciton diffusion length.

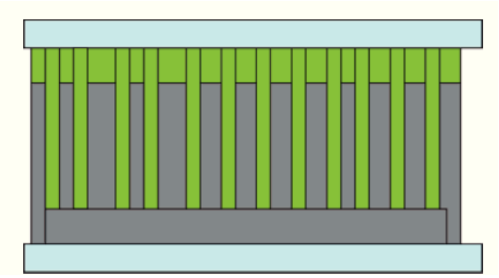

Figure 3.6.1. Schematic architecture of a photovoltaic device combined with BHJ and bilayer structure. The D and A phases should be ideally in the nanoscale comparable with the exciton diffusion length.

Interdigitated phases have to be organized in percolated highways to ensure high mobility charge carrier transport and reduced recombination. Moreover, there should be two pure donor and acceptor phases at collecting electrodes in order to minimizes the losses by recombination of the wrong sign of charges at the wrong electrode, as well as acting as diffusion barriers for the wrong sign charge carriers. Due to the disorder in polymer mixture such a well-organized nanostructure is not easy to obtain.

3.7 Post production treatments

As it has been mention before, morphology of the active layer of BHJ thin films is one of the most important factors in solar cell performance optimization. In the last years a lot of effort has been put to control the nanostructure of the plastic solar cells.

The morphology is strongly affected by the processing conditions such as:

- Vapour pressure of solvent [41,42];
- The rate of solvent removal [43];

- The volume fractions of the components [44]; or
- the use of chemical additives [45,46].

But to achieve high efficiently organic solar cells, a post production treatment is required. The most popular and commonly used is a thermal treatments called ***annealing*** [47,48]. There has been a tremendous amount of research performed to understand the influence of the temperature on the BHJ solar cells based on P3HT-PCBM blends [49-51].

It has been reported that:

- When a polythiophene is annealed to a temperature higher than its glass transition temperature, an enhance crystallization of the polymer take place [52].
- Along with this enhanced crystallization of the polymer, the hole conductivity of the P3HT increases dramatically [53].
- During the heat treatment the polymer chains are more mobile [54].
- Annealing enhance interpenetration donor-acceptor networks and PCBM crystalline domains are formed, providing better exciton harvesting and charge transportation.
- With enhance crystallinity of the composite, there can be better percolation of charges by reducing internal resistance.

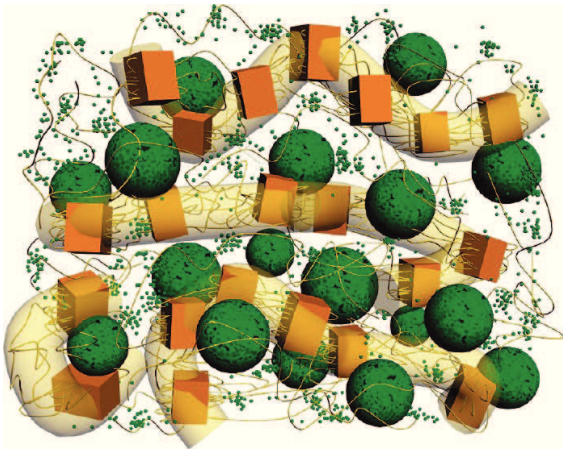

Figure 3.7.1. Cartoon for a thermally annealed P3HT/PCBM film. The intercalated PCBM aggregates (large spheres) and P3HT crystallites (blocks) are immersed in the matrix of P3HT amorphous chains (thin wires) and dispersed PCBM molecules (small spheres) [55].

As a result perfect conditions for the fabrication of devices based on P3HT-PCBM has been found. PCE of 4% can be obtain with film of P3HT-PCBM dissolved in chlorobenzen with the weight ratio c=1:0.8, film thickness around 120 nm, and thermal annealing at 120-160°C for 5-30 min; processing detail determine that these parameters fluctuate in a certain range [56].

However, the use of high temperatures is not ideal for fabrication on flexible, plastic substrates for which maximum temperatures well below 100 °C are desirable. For this reason continuous research is carried to find better solution.

A potential alternative to thermal treatments is the application of ***an external electric field*** during the film formation that supports the self-organization of the polymer.

It is known that:

- P3HT is a polar molecule with a dipole moment of ~1.0–1.6D polarity comes mainly because of the presence of an electronegative sulfur atom in the heterocycle ring [57].

- Simultaneous application of an external electric field will try to align the polar dipoles in the direction of the electric field, which is known as "dipole polarization," leading to more oriented polymer chain[58].

- It is presumed that electric field support an orientation of the polymer chains inside the photoactive matrix in the direction of the electric field.

- A simultaneously applied external electric field greater that the Voc of the device injects (additional) charges into the polymer bulk.

3.8 A standardized procedure

It may be difficult to compare results from different laboratories around the world since there is no standardized lifetime test.

There are several aspects that make quantitative comparison virtually impossible between different studies (e.g., incident light intensities, under continuous or intermittent illumination, in the dark, encapsulated, in inert atmosphere, in air, outside under real conditions, at different temperatures, at specified or unspecified levels of humidity). To conclude, a standardized method of reporting data would not only be useful but it is of great importance for further development of the field.

A group of Krebs [58] proposed a list of parameters that should be specified and addressed in the measurements:

- **Light:**
  - Source (solar simulator, halogen lamp, tungsten,laser source, real sun).
  - Intensity and intensity measurement (bolometric,silicon diode).
  - Spectrum and filters (AM1.5G, AM1.5D, spectrum analyzer).
  - Conditions (continuous, intermittent, intensity variation, dark storage).

- **Electrical measurement:**
  - Source measure unit and connection to the cell.
  - Conditions (IV-curves, Jsc, Voc, conditions between measurements).
  - Number of measurement points, step speed and direction.
  - Total charge and total energy generated by the cell.

- **Temperature:**
  - Measurement (surface, substrate, surroundings).
  - J Heating/cooling means (air circulation, solid contact heat transfer).

- **Atmosphere:**
  - Ambient, vacuum, inert, glovebox (ppm levels of O2 and H2O).
  - J Humidity (humidity level, humidity control).

- **Device conditions:**
  - Solid substrate, flexible substrate, encapsulation,active area.
  - Electrical contacts (point contact, epoxy glue).

- **Field testing:**
  - Outdoor–indoor, day/night cycles.
  - Weather conditions.

Further, the availability of complete instrumental packages would facilitate the comparing activity and eventually further developments.

References

[1] J. Nelson, in *The Physics of Solar Cells*, Imperial College Press, London, **2003**

[2] C .J. Brabec, in *Organic Photovoltaics. Concepts and Realization*, Springer-Verlag, Heidelberg, **2003**, 159

[3] O. Inganäs, L. Stoltz Roman, in *Organic Photovoltaics. Concepts and Realization*, Springer-Verlag, Heidelberg, **2003**, 249

[4] V.D. Mihailetchi et al, *J. Appl. Phys.* **2003,** *94*, 6849.

[5] C. Brabec et al, *Thin Solid Films* **2002,** *403-404*, 368.

[6] M.M. Mandoc et al, *Adv. Funct. Mater.* **2007,** *17*, 2167.

[7] L.J.A. Koster et al, *Appl. Phys. Lett.* **2006,** *88*, 93511.

[8] N. S. Sariciftci et al., Chem. Rev. **2007,** 107, 1324-1338

[9] C.J. Brabec et al, *Appl. Phys. Lett.* **2002,** *80*, 1288.

[10] S.K.M. Jonsson et al, *Jpn. J. Appl. Phys. 1* **2005,** *44*, 3695.

[11] E. Ahlswede et al, *Appl. Phys. Lett.* **2007,** *90*, 163504.

[12] T. Nyberg, *Synth. Met.* **2004,** *140*, 281.

[13] K. Tvingstedt et al, *Appl. Phys. Lett.* **2007,** *91*, 123514.

[14] G.-M. Ng et al, *Appl. Phys. Lett.* **2007,** *90*, 103505.

[15] G. Dennler et al, *Appl. Phys. Lett.* **2006,** *89*, 073502.

[16] J. Gilot et al, *Appl. Phys. Lett.* **2007,** *90*, 143512.

[17] C.W. Tang, *Appl. Phys. Lett.* **1986,** *48*, 183.

[18] S.A. Jenekhe, S. Yi, *Appl. Phys. Lett.* **2000,** *77*, 2635.

[19] M. Granstrom et al, *Nature* **1998,** *395*, 257.

[20] N.S. Sariciftci et al, *Appl. Phys. Lett.* **1993,** *62*, 585.

[21] D.E. Markov et al, *J. Phys. Chem. A* **2005,** *109*, 5266.

[22] L.A.A. Pettersson et al, *J. Appl. Phys.* **1999,** *86*, 487.

[23] J.J.M. Halls et al, *Appl. Phys. Lett.* **1996,** *68*, 3120.

[24] A. Haugeneder et al, *Phys. Rev. B: Condens. Matter* **1999,** *59*, 15346.

[25] T. Stubinger, W. Brutting, *J. Appl. Phys.* **2001,** *90*, 3632.

[26] O. Inganäs et al, *Synth. Met.* **2001,** *121*, 1525.

[27] L. Chen et al, *Adv. Mater.* **15,** *12*, 1367.

[28] M. Drees et al, *Phys. Rev. B: Condens. Matter* **2004,** *69*, 165320.

[29] G. Yu, A.J. Heeger, *J. Appl. Phys.* **1995,** *78*, 4510.

[30] G. Yu et al, *Science* **1995,** *270*, 1789.

[31] C.Y. Yang, A.J. Heeger, *Synth. Met.* **1996,** *83*, 85.

[32] C.J. Brabec et al, *Adv. Funct. Mater.* **2001,** *11*, 15.

[33] P.W.M. Blom et al, *Adv. Mater.* **2007,** *19*, 1551.

[34] F. Yang et al, *Nat. Mater.* **2005,** *4*, 37.

[35] T. Martens et al, *Appl. Phys. A* **2004,** *79*, 27.

[36] H. Liu et al, *Adv. Funct. Mater.* **2001,** *11*, 420.

[37] X. Yang et al, *Nano Lett.* **2005,** *5*, 579.

[38] V.D. Mihailetchi et al, *Adv. Funct. Mater.* **2006,** *16*, 699.

[39] S.M. Tuladhar et al, *Adv. Funct. Mater.* **2005,** *15*, 1171.

[40] A. Gadisa et al, *Org. Electron.* **2006,** *7*, 195.

[41]S. E. Shaheen et al, *Appl. Phys. Lett*. **2001**, 78, 841–843.

[42] S.H. Park et al, *Nat. Photonics* **2009**, 3, 297–303.

[43] G. Li et al, *Nat. Mater*. **2005**, 4, 864–868

[44] A.C. Mayer et al, *Adv. Funct. Mater.* **2009**, 19, 1173–1179.

[45] A. Pivrikas et al, *Org. Electron.* **2008**, 9, 775–782.

[46] J. Peet et al, *Nat. Mater.* **2007**, 6, 497–500.

[47] W.L. Ma et al,. *Adv. Funct. Mater.* **2005**, 15, 1617–1622.

[48] H. Hoppe; , N.S.J. Sariciftci. *Mater. Chem*. **2006**, 16, 45–61.

[49] Y. Zhao et al, *Appl. Phys. Lett.* **2007**, 90, No. 043504

[50] J. Jo et al, *Adv. Funct. Mater*. **2009**, 19, 2398–2406.

[51] S.S. Van Bavel et al, *Nano Lett* **2009**, 9, 507–513.

[52] L.Y.Zhao et al, *Polymer* **1995**, 36, 2211.

[53] T.Lee, O.O. Park, *Appl.Phys.Lett*. **2000**, 77, 3334.

[54] J.J. Dittmer et al, *Adv.Mater.* **2000**, 12, 1270.

[55] W. Wu et al., *ACS Nano* **2011***,* 5, 8, 6233-6243.

[56] W. Ma et al, *Adv. Funct. Mater*. **2005**, 15, 1617–1622.

[58] F. C. Krebs, *Solar Energy Materials & Solar Cells,* **2008**, 92, 686-714.

[57] C. F. N. Marchiori, M. Koehler *Synthetic Metals,* **2010,**160,643-650.

[58] Y. Li et al, *Synthetic Materials,* **2008**, 158, 190-193.

4 P3HT-PCBM blend

4.1 Introduction

Organic solar cells based on light-harvesting mixtures of electron donor and acceptor materials offer a promising route toward the development of lightweight, cost-effective, large-area, flexible organic photovoltaic solar cells.

A milestone in the development of OSCs was the fabrication of a bilayer heterojunction with an efficiency approaching 1% by Tang in 1986 [1]. He recognized the fact that the performances of bileyer heterojunction are limited by the short exciton diffusion length in organic materials (typically 10-20 nm). The exciton dissociation process is limited to the donor-acceptor interfacial zone, so only excitons produced at a distance shorter than their diffusion length have a good probability to reach the interface and generate free charge carriers. Consequently, the exciton diffusion length limits the thickness of the active layer and thus

the maximum fraction of the incident light that the cell can absorb and convert into electricity. Bilayer heterojunction devices are still intensively investigated as they are a priceless tool for the evaluation of new active materials.

An efficient way to bypass this problem consists of the realization of interpenetrated networks of the donor and acceptor materials called ***bulk heterojunction (BHJ)***. A huge extension of the interface between the donor and acceptor materials leads to a considerable increase of the number of excitons dissociated and hence of the conversion efficiency of the cell [2].

Sariciftci et al. in 1992, demonstrated that photoexcitation of a mixture of a poly-(*p*-phenylenevinylene) derivative and C_{60} fullerene lead to ultrafast photo induced electron transfer at a donor-acceptor interface [3]. The long lifetime of the charge-separated state related with the delocalization of the charges over the π-conjugated system and fullerene group respectively allow both efficient charge transport and charge collection at the electrodes [2].

Fullerenes and in particular soluble C_{60} derivatives [6,6]-phenyl-C_{61}-butyric acid methyl ester (PCBM) (figure 4.1.1) have been a key component for the development of BHJ solar cells [4].

The first prototypes of BHJ cells were based on polymers of the PPV series [2]. In recent years, these polymers have been replaced by regioregular poly(3-hexylthiophene) P3HT (figure 4.1.1), which presents the advantages of:

- a lower band gap and
- higher hole mobility [5-7].

Within a relatively short period P3HT has become the archetype donor for BHJ cells and power conversion efficiencies of 5% have been recently reported [5-7].

The performance of BHJ devices depends on the morphology of the active layer [8] and it is a challenge to maximize absorption of photons, separation and transport of charges while maintaining the necessary size scale and continuity constraints of the morphology of these blends. Added to this is the segregation of components at the interface between the active layer and cathode/anode to facilitate electron/hole collection and minimize charge carrier recombination. In addition, the thickness of the active layer, usually ~ 100-200 nm, confined between the two electrodes interfaces place constraints on the morphology development [9].

Here we present studies based on P3HT and PCBM blends with different preparation conditions which strongly affect and influence on the morphology and efficiency of OPVs devices. Various processing conditions such as: thermal annealing treatment, deposition rate, slow and fast cooling and ultrasonically treated blend has been investigated.

4.2 P3HT

Poly(3-hexylthiophene-2,5-diyl) (P3HT) is a conjugated polymer, see figure 4.2.1. It is a commonly used polymer in organic solar cells and acts as the light absorbing and hole transporting material. P3HT has a high solubility and due to the alkyl-groups a high potential crystallinity. The degree of crystallinity is affected by the regioregularity of the polymer. A regioregular P3HT usually has a regioregularity of minimum 90 %. The higher the regioregularity, the higher the cristallinity. It was also recognized that higher molecular weight leads to a red shift in the absorbtion spectrum and to higher hole mobility [10,11].

P3HT is a conjugated polymer with a thiophene backbone. The carbon atoms in the thiophene rings are sp2 hybridized, and thus form a π-bond with the neighbor carbon atoms. In the polymer the π-bonds form

a π-band which is called the highest occupied molecular orbital (HOMO). In this π-band the electrons are delocalized. The bandgap of thiophenes is build by transition from the aromatic into the quinoid structure. Impurities in the polymer act like a p-type doping are giving pure P3HT a electrical conductivity.

The used P3HT is from Sigma-Aldrich and has a regioregularity of at least 90 %. The average molecular weight is 50000 g/mol. The LUMO level is 3.2 eV and the HOMO level is at 5.1 eV [13]. The hole mobility in P3HT depends on different factors and lies between 10^{-5} and 10^{-2} $cm^2/V*s$ [12]. The electron mobility is negligible small [13].

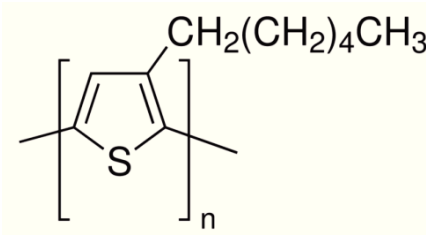

Figure 4.2.1. Chemical structure of Poly(3-hexylthiophene-2,5-diyl) P3HT.

4.3 PCBM

Phenyl-C61-butyric acid methyl ester (PCBM) is a fullerene based molecule (figure 4.3.1). It contains a Bucky-ball (C60), and to make it soluble the methyl-ester group is attached. PCBM is a n-type material and can take up to six electrons. It also has a π-band, but the electrons are moving in the π*band, or LUMO. The mobility in PCBM is between $2*10^{-3}$ and $2*10^{-2}$ cm^2=V*s [13]. The hole mobility is negligible small.

In this thesis the PCBM from Solenne 99 % is used.

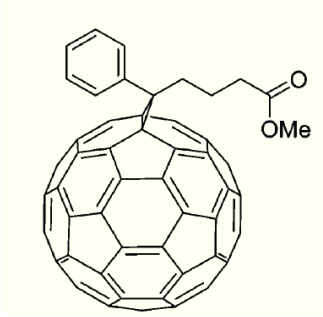

Figure 4.3.1. Chemical structure of phenyl-C61-butyric acid methyl ester PCBM.

4.4 P3HT-PCBM

Among conjugated polymers P3HT has been most widely used polymer as electron donor along with PCBM as electron acceptor. We studied performance of devices based on blend of P3HT and PCBM.

The energy level of the highest occupied molecular orbital (HOMO) was determined by cyclic voltammetry (CV) measurements. This was conducted by Dima in the labs of Dr. Daren Caruana (UCL-Chemistry). The energy level of the lowest unoccupied molecular orbital (LUMO) was calculated using the energy gap calculated from the corresponding UV/Vis spectra of the IR-polymers in solution (figure 4.4.1).

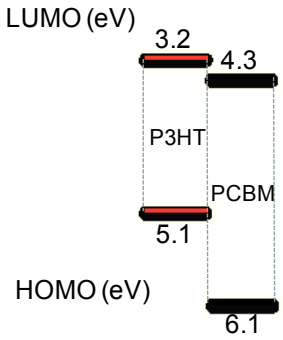

Figure 4.4.1. Energy levels of P3HT and PCBM.

A LUMO level allowing efficient photoinduced charge transfer from the donor, the spherical geometry of C_{60} leads to isotropic electron transport through a 3D percolation system, which seems particularly appropriate for charge transport in disordered media.

In figure 4.4.2 can be seen the absorbance of P3HT, PCBM and P3HT-PCBM blend in solution of chlorobenzene. The main absorption peak of P3HT appear in the visible region at approximately 510, 545 and 600 nm, while those of PCBM appear in the UV region at approximately 305 and 335 nm. Whereas the absorption peak of the blend appear at approximately 330 and 490 nm.

Having a band gap of ~1.90 eV and a rather narrow absorption band (fwhm~150nm), P3HT can absorb only a limited fraction of the solar photons (~30%). Relatively high-lying HOMO level sets the maximum cell voltage to 0.60-0.65 V and represents a potential cause of instability in atmospheric conditions.

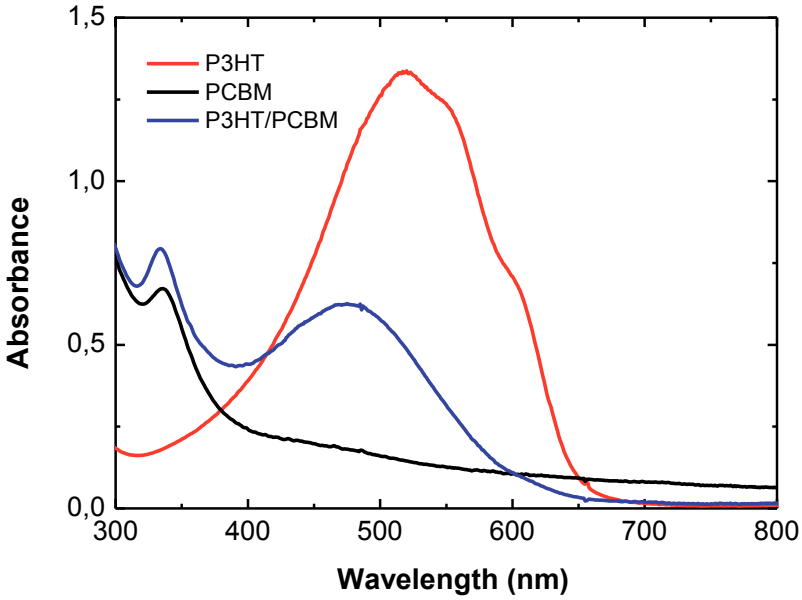

Figure 4.4.2. Absorbance of P3HT, PCBM and P3HT-PCBM blend dissolved in chlorobenzen.

4.5 Solution preparation

P3HT and PCBM were dissolved in chlorobenzene separately, with a concentration of 22 mg/ml each (2% wt) and then stirred in air and heated at temperature of ~70° over night. Solutions were then mixed together in ratio P3HT:PCBM=1:0,8. Successively, the solution was portion, and different treatments were applied. First portion was stirred for about 3 hours before the deposition. Second part was stired and ultrasonicated for 3 hours to get a homogenous blend.

4.6 Device preparation

Devices were produced in the following structure (Figure 4.6.1):

ITO / PEDOT:PSS (~80 nm) / active layer (~120 nm) / Al (150 nm)

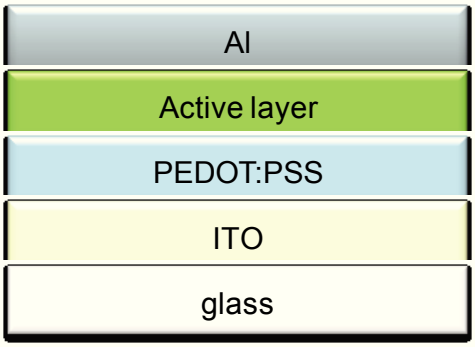

Figure 4.6.1. Schematic structure of the device.

1. Indium tin oxide (ITO) substrates were ultrasonically cleaned with acetone and isopropanol for 15 min each before being subjected to the O_2 plasma treatment for 15 min.

   Indium tin oxide is a transparent conductive oxide. In an organic solar cell at least one electrode has to be transparent in order to absorb the light in the active layer. It is quite common in opto-electronics to use ITO. In this thesis the ITO was bought already on the glass from Visiontek Systems. It has a sheet resistance of 15 Ωsq. The AFM image of surface topography of the ITO is presented on figure 4.6.2.

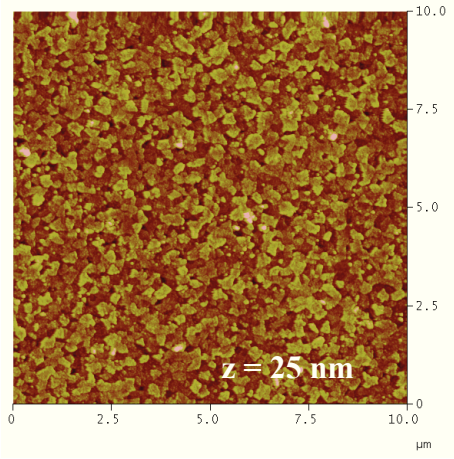

Figure 4.6.2. AFM image of topography of the ITO surface.

2. PEDOT:PSS poly(3,4 ethylendioxythiophene)-poly(styrenesulfonate) was filtered (0.45 µm) and then spin-coated in air on the top of the clean ITO substrates immediately after the O_2 plasma treatment at a speed of 4000 rpm for 60 s. The resulting thickness of the layer was about 80 nm.

   PEDOT:PSS is a conducting conjugated polymer which is used to improve the extraction properties between the ITO and the P3HT and to smooth out the ITO film. The layer thickness is usually less than 100 nm and thus transparent. In this thesis the PEDOT:PSS VP AI 4083 from Sigma-Aldrich is used, which has a work function of 4.8-5.2 eV.

3. After annealing the PEDOT:PSS for 15 min at 140 °C on a hot-plate inside the nitrogen glove-box a thin layer of the P3HT/PCBM solution was spin-coated on the top-surface at different speed 800 rpm, 900 rpm, 1200 rpm, 1500 rpm. The resulting thickness range was between 170 and 120 nm.

4. Finally, aluminium electrodes were thermally evaporated on top of the organic active layer under high vacuum conditions at an evaporation rate of 2 Å/s forming a layer of the aluminium of 150 nm. The base pressure during the evaporation was $4*10^{-6}$ mBar. About 0,8 kA of aluminium was pre-evaporate before the proper evaporation.

5. The devices were completed by thermal annealing on a hot plate at different temperatures 140 °C and 180 °C, inside the nitrogen-filled glove box. Two different ways of cooling (slow and fast) after annealing, were investigated.

4.7 Characterization

Devices with an active area of 14 mm^2 were characterized by current-voltage (J-V) measurements in vacuum by using a Keithley 2400 source unit under AM1.5 conditions with illumination of 100 mW/cm^2.

The incident-photon-to-converted-current efficiency (IPCE) was measured with the help of solar simulator Sun 3000 110*110 mm, Abet Technologies.

Thicknesses were measured using a Dektak surface profilometer.

All atomic force microscopy (AFM) images have been recorded in tapping mode using a Veeco Instruments NanoScope Dimension 3100.

4.8 Results and discussion

In general, it is necessary to optimize production parameters to obtain good solar cells. Here we investigated influence of: spin speed deposition rate of the active layer, thermal annealing temperature, slow and fast cooling rate of the active layer and ultrasonication of the blend of donor-acceptor materials before the deposition, on the performance of the devices

4.8.1. J-V curve

Figure 4.8.1.1 show the J-V curve characteristics under AM 1.5 illumination for a calibrated solar simulator with an intensity of 100 $mW*cm^{-2}$. Different spin speed deposition of the active layer were investigated. All devices were annealed at the same conditions (140 °C for 10 min).

The highest efficiency of 3.08 % was obtained from the devices where the active layer was deposited with the spin speed of 800 rpm, giving Jsc of 8.85 mA/cm^2, Voc of 0.60 V and FF of 0.58; see table 1. The active layer deposited with this spin speed gives the film thickness of 170 nm which results optimum for this kind of devices. In conclusion the efficiency of the device is depending on the thickness of the active layer which can optimize the absorption of photons and the transportation of the charge carrier.

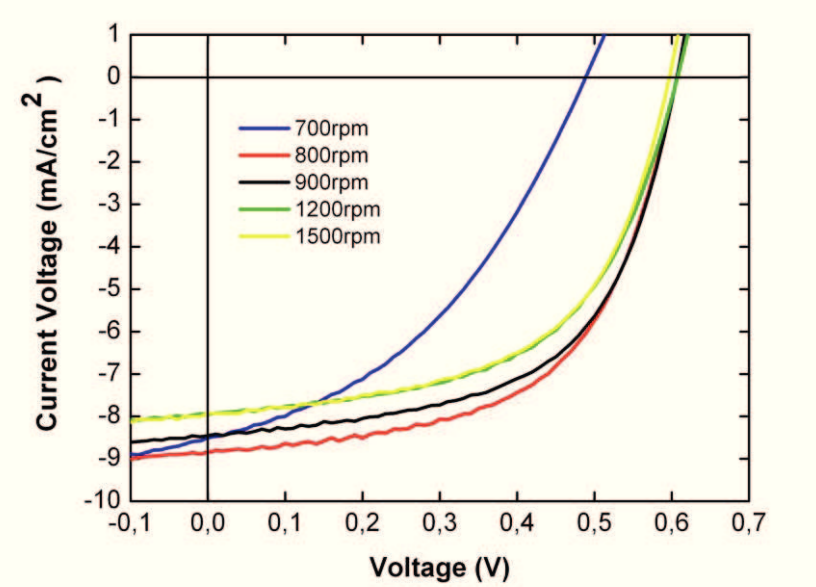

Figure 4.8.1.1. J-V curve characteristic of P3HT-PCBM devices for different spin speed deposition of the active layer.

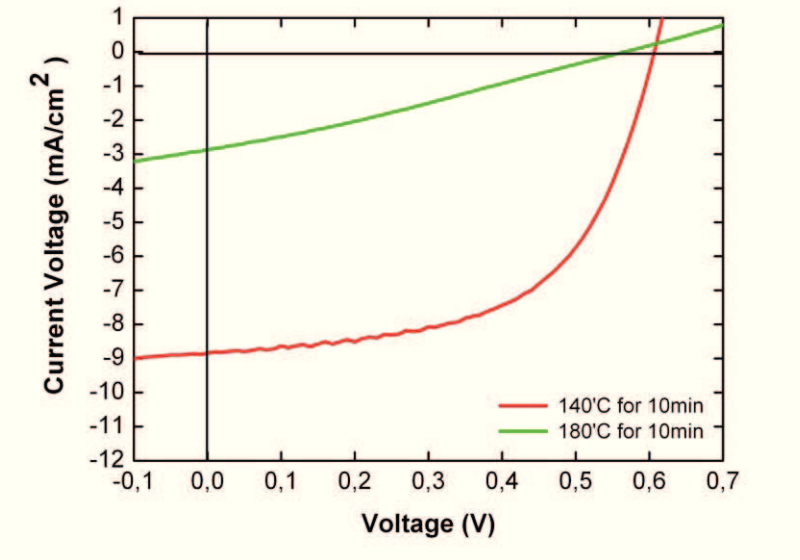

Figure 4.8.1.2. J-V curve characteristic of P3HT-PCBM devices for two different thermal annealing temperatures.

Subsequently we studied the influence of two different annealing temperatures (140 °C and 180 °C) on the performance of the devices deposited with spin speed on 800 rpm which we found the optimum for our devices. Figure 4.8.1.2 show the J-V curve characteristics under AM 1.5 illumination for a calibrated solar simulator with an intensity of 100 mW*cm^{-2}. Annealing cause the phase separation, but after to high temperature the phase separation is too big , so we obtain small interface. At elevated temp the PCBM molecules can diffuse thought P3HT and form large crystals which decrease the photovoltaics properties.

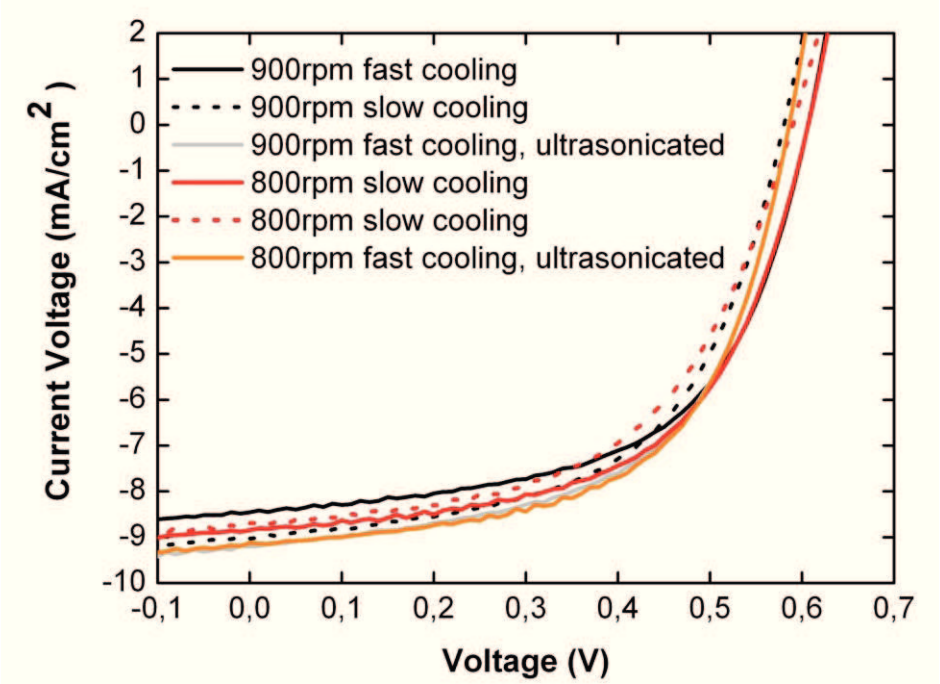

Figure 4.8.1.3. J-V curve characteristic of P3HT-PCBM devices for different treated blend solution and different cooling rate anneled at 140°C for 10min.

Afterwards another two parameters were studied. Cooling rate of the active layer, and ultrasonicated treated blends of the donor-acceptor materials, before the deposition. Figure 4.8.1.3 show the J-V curve characteristics under AM 1.5 illumination for a calibrated solar simulator with an intensity of 100 mW*cm^{-2}. The first parameter shows that devices prefer to be treated by fast cooling after annealing. It has been observed that ultrasonication has positive influence on the performance of the devices giving IPCE of 3.15% Jsc of 9.13 mA*cm^2, FF of 0.60 and Voc of 0.58. It seems that ultrasonication helps to homogenous the blend, which helps in the film formation.

Table 4.1. Photovoltaic properties of the organic photovoltaic cells based on P3HT-CBM blend under different preparation conditions.

Parameters		Jsc (mA/cm^2)	Voc (V)	FF	IPCE (%)
deposition rate	1500 rpm	7.96	0.59	0.56	2.67
	1200 rpm	7.95	0.60	0.56	2.68
	900 rpm	8.46	0.60	0.59	2.97
	800 rpm	8.85	0.60	0.58	3.08
	700 rpm	8.51	0.48	0.41	1.69
annealing temperature	180 °C	2.87	0.60	0.28	0.45
	140 °C	8.85	0.59	0.58	3.08
cooling rate for spin speed deposition 800rpm	Fast	8.85	0.60	0.58	3.08
	Slow	8.82	0.58	0.55	2,79
	slow with ultrasonication	9.13	0.58	0.60	3.15
cooling rate for spin speed deposition 900rpm	Fast	8.43	0.60	0.59	2.97
	Slow	9.00	0.57	0.57	2.95
	slow with ultrasonication	9.20	0.58	0.59	3.11

4.8.2. AFM images of P3HT-PCBM blend

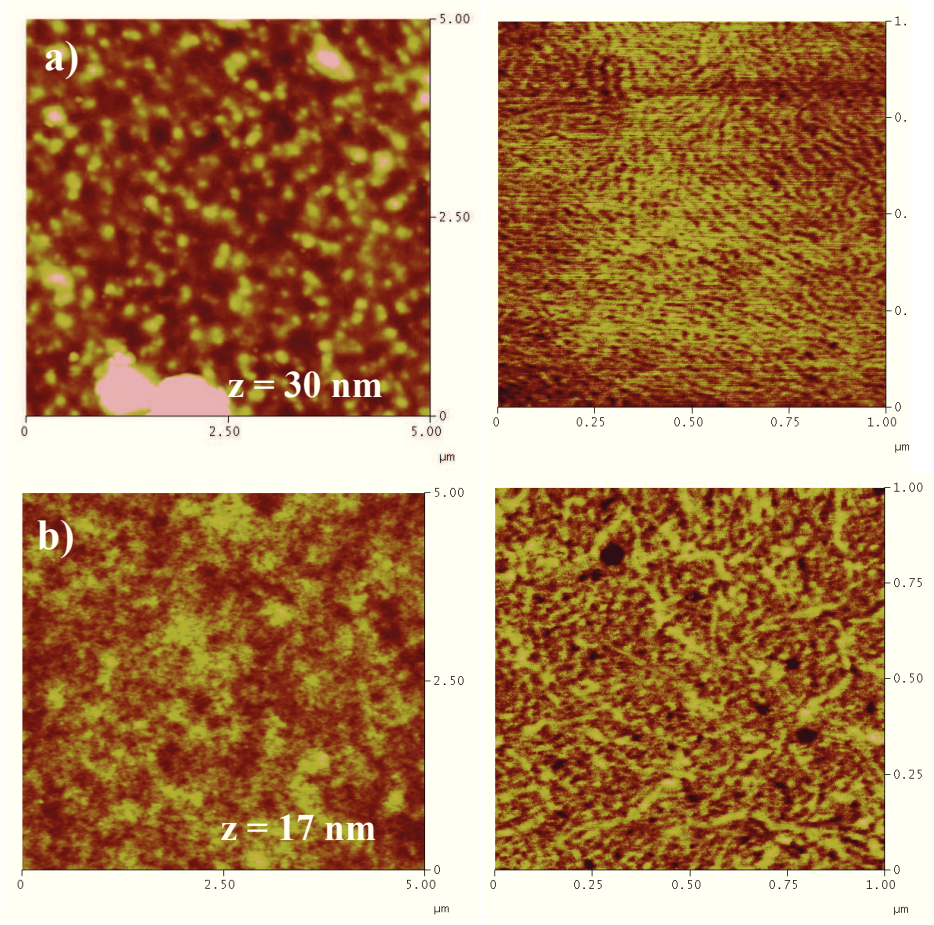

Figure 4.8.2.1. AFM images (left: topography, right: phase) of the active area of P3HT-PCBM blend; a) before, b) after annealing on 140°C for 10 min.

AFM images of the P3HT-PCBM films before and after annealing, are shown in figure 4.7.2.4. Without any heat treatment, the interpenetrating networks are not well developed, and donor-acceptor domains are difficult to distinguish. After thermal annealing for 10 min

on 140°C, the morphology of the interpenetrating DA networks becomes clearer and easily visible with typical feature size of ~10 nm. The changes in morphology result in a large interfacial area for efficient charge generation. Temperature of annealing also improves the crystallinity within the phase-separated networks and thereby facilities charge transport to the electrodes. The AFM analysis of the images indicated that one phase is a pure P3HT crystal domain and the other phase is the mixture of amorphous P3HT and PCBM, which is not consistent with a phase separation of the components by a spinodal decomposition mechanism.

4.9 Conclusions

In conclusions, we have fabricated P3HT and PCBM bulk heterojunction solar cells. Device performance were studied with different preparation conditions. Different thermal annealing temperature, spin speed deposition of the photoactive layer, cooling rate and ultrasonicated treated blend were studied. Nanostructed morphology of the P3HT-PCBM was investigated and confirm with AFM analysis. Devices show the best performance when the blend of the donor-acceptor material is treated with ultrasounds before the deposition, which result in more homogenous film, with annealing temperature at 140 °C for 10 min and slow cooling afterwords. Organic solar cells gives IPCE of 3.15% Jsc of 9.13 mA*cm^2, FF of 0.60 and Voc of 0.58. The high efficiency can be explained by the ability of the blend of P3HT-PCBM to phase separate and crystallize into desirable BHJ morphologies after processing, allowing for efficient charge separation and transport. AFM analysis show the formation of elongated PCBM nanocrystals provides efficient percolation paths for the electron thereby improving device performance.

Reference

[1] C. W. Tang, *Appl. Phys. Lett.,* **1986**, *48*, 183–185.

[2] C. J. Brabec et al, *Adv. Funct. Mater.,* **2001**, *11*, 15–26.

[3] N. S. Sariciftci et al, *Science,* **1992**, *258*, 1474–76.

[4] J. C. Hummelen, et al, *J. Org. Chem.,* **1995**, *60*, 532–538.

[5] G. Li et al, *Nat. Mater.,* **2005**, *4*, 864–868.

[6] W. Ma et al, *Adv. Funct. Mater.,* **2005**, *15*, 1617–1622.

[7] M. Reyes-Reyes et al, *Appl. Phys. Lett.,* **2005**, *87*, 083506.

[8] S. Ghosh et al, *Appl. Phys. Lett.*, **2008**, 92, 151911.

[9] D. Chien et. al., *Nano Lett.,* **2011**, 11, 561–567.

[10] A. Zen et al, *Adv. Funct. Mater*., **2004**, 14, 757.

[11] P. Schilinsky et al, *Chem. Mater.*, **2005,** 17, 2175.

[12] A. Mozer et al, *Physical Review*, **2005**,71, 352141-352149.

[13] J. Nakamura et al, *Appl.Phys. Lett.,* **2005,** 87, 132105.

5 External electric field

5.1 State of the art

Polymer solar cells based on poly(3-hexylthiophene) (P3HT) and fullerene derivative phenyl-C61-butyric acid methyl ester (PCBM) have attracted great interest for fabricating:

- low-cost,
- large areas,
- solutions processing,
- easy manufacture and
- flexible photovoltaic devices [1-4].

For these kind of cells, a power conversion efficiency of about 5% [5] has been reported. Due to the short exciton diffusion length (10nm) of a semiconducting polymer, the electron acceptors are usually

mixed with polymers (electron donor) to form a bulk heterojunction (BHJ) structure [6,7].

The performance of such devices and the efficiency in particular strongly depend on *the morphology of the active layer* [8], which, in turn, influences the charge-extraction process in P3HT-PCBM solar cells. While several approaches have been used to improve the PCE of polymeric solar cells *by controlling the nanoscale morphology* of P3HT-PCBM blends but relatively high-temperature ($130 < T < 155$ °C) thermal treatments, are usually acknowledged to be the most effective [12-14].

It would be technologically favorable to develop deposition process which can be implemented at low temperatures for the future industrial production. A potential alternative to thermal treatments is the application of an electric field during the film formation supports the self-organization of the polymer. Padinger and co-workers were the first who investigated the influence of the electric field on BHJ solar cells, showing an improvement by a factor of 1.4 in the device performance [9]. Later on, a group of Jin et al. has been studying the influence of the electric field on the MEH-PPV- fullerene composite devices during spin-coating of the active layer, showing an enhancement by a factor of 1.7 in the performance of this devices external quantum efficiency (EQE) [10]. Lin and co-workers presented an application of the external electric field during the annealing of solvent suggesting that, electric field-assisted annealing facilitates the crystallization of P3HT improving carrier transport and photovoltaic performance up to 4 % [11]. Kumar et al. has presented another approach which enables a simultaneous anneal and apply an electric field under the vacuum for one hour resulting enhanced by a factor of 2.5 in PCE [12].

However, these processes need a long period of annealing that leads to the aggregation of PCBM and reduces the lifetime and performance of the devices [13].

Not much work has been done toward the definition of fabrication processes which could be implementable at *low temperature.*

In this chapter it is presented a simple and fast method of application of a DC electric field on completed encapsulated devices aiming to show that high annealing temperatures can be avoided from the production of plastic solar cells. I present a comparison between P3HT-PCBM based BHJ solar cells where an electric field was applied with and without thermal post-treatment. Results show that increasing the applied voltage during the electric field treatment leads to PCEs similar to the ones obtained when also a thermal treatment is simultaneously applied as also that the electric field method can provide a new route to fabricate large-area polymer solar cells at low temperatures.

5.2 Device preparation

P3HT and PCBM were dissolved in chlorobenzen separately, with a concentration of 20 mg/ml each, and then mixed together with a ratio 1:0,8.

1. Ossila's pre-patterned indium tin oxide (ITO) substrates [14] were first ultrasonically cleaned, using acetone and isoproponal for 15 min each, and then subjected to an O_2 plasma treatment for 10min [15,16] to remove the protective photoresist layer, clean the surface and increase the work function of ITO before the deposition. Each substrate has six individual pixels and a cathode connection strip.

2. On top of the substrate poly(3,4-ethylenedioxylenethiophene) (PEDOT:PSS) in aqueous solution, was immediately spin-coated

at a speed of 4000 rpm (rounds per minute) to form a 80 nm thick film and then wipe free the cathode strip afterwards. Successively, substrates were annealed in a nitrogen-filled glove-box for 15 min at 150°C.

3. The P3HT:PCBM blends were spin-coated at 900 rmp, yielding films with thickness ~150 nm and the cathode strip were wipe again.

4. After the deposition, 150 nm of Al were thermally evaporated on top inside a vacuum chamber (10^{-6} Torr).

5. Subsequently, devices were encapsulated by simply placing a drop of UV-cured epoxy glue on the device and placing the glass cover slip on top before curing under UV-lamp for approximately 30 minutes.

6. Devices were completed by adding connection legs with a standard 0.1" (2.54 mm) pitch (see Figure 5.2.1).

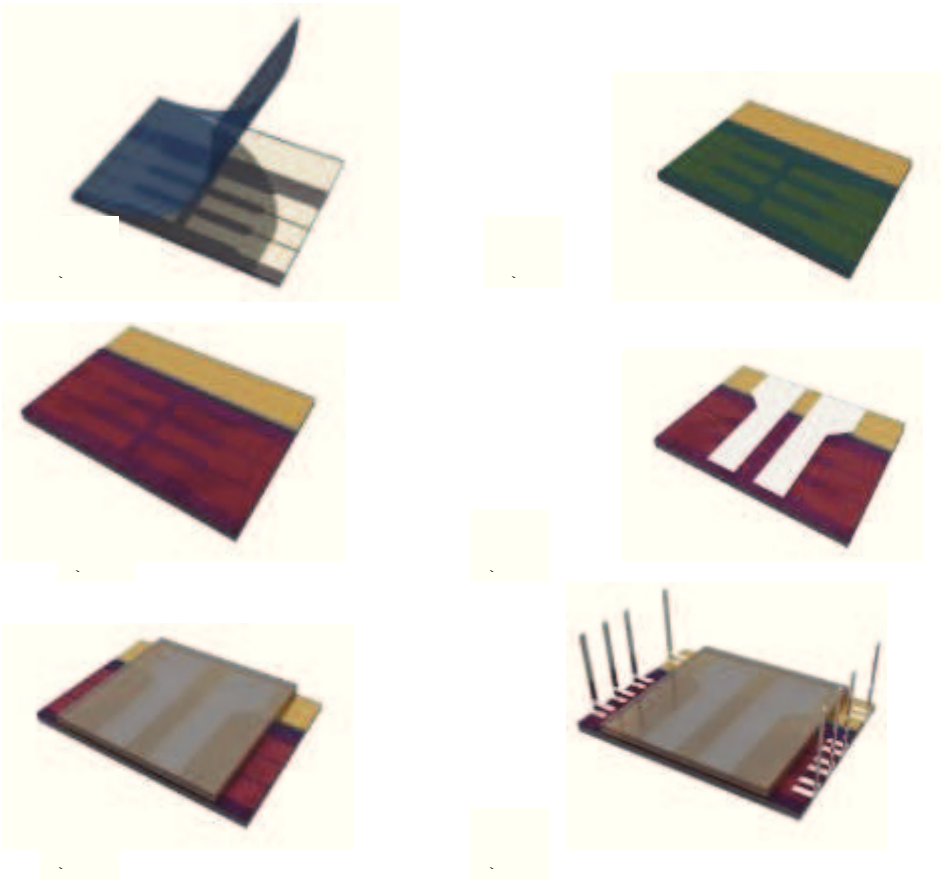

Figure 5.2.1. Fabrication of the encapsulated devices, a) cleaning and an O_2 plasma treatment , b) depositions of PEDOT:PSS, c) deposition of the active layer, d) thermal evaportion of aluminium electrode, e) encapsulation, f) final device with added conecction legs.

Finally, part of the devices were further treated by annealing and simultaneously applying an external electric field. Devices were placed on a hotplate while a potential difference was applied between the electrodes for several minutes (see Figure 5.2.2). Afterwards, devices were cooled to room temperature before measurements were started. The

remaining part of the devices were treated by the mean of the external electric field only.

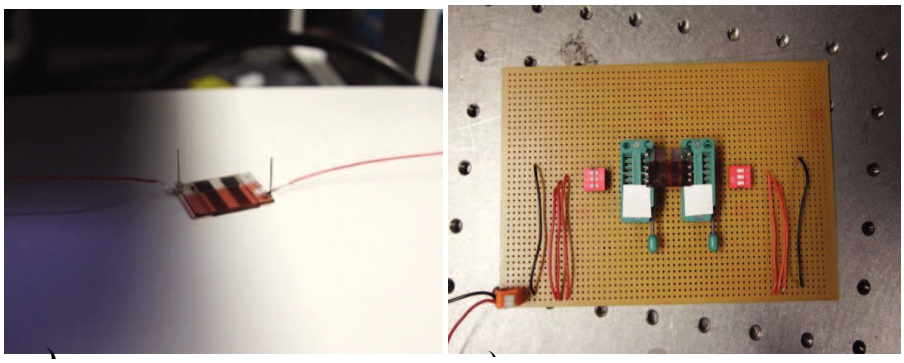

Figure 5.2.2 Laboratory experiments, devices during postproduction treatment where a) heat and DC were applied simultaneously, b) only DC were applied. Picture of our prototype board for measurements encapsulated devices.

5.3 Characterization

All devices were illuminated through ITO electrodes through the glass cover slip. Current-voltage (J-V) measurements were carried out by a Keithley 2400 source unit and our prototype board (with allowed electrical connection to the six individual pixels), under AM1.5 solar simulator with illumination of 100 mW/cm^2. Thicknesses were measured using a Dektak surface profilometer.

5.4 Results and discussion

Figure 5.4.1 shows the current-voltage behaviour of P3HT:PCBM solar cells under illumination with white light at an irradiation intensity of 100 mW/m^2. Devices were treated at 140 °C under different forward

bias from 2, 5, 8 to 12 V, for 2 and 10 min (marked lines). Table 5.1 lists the parameters and the characteristic for this devices.

The figure shows the photovoltaic element without any postproduction treatment (straight line). Electrical characteristics of this device are: open circuit voltage, Voc~0.58 V; short circuit current density, J_{sc}~6.17 mA/cm^2; and fill factor, FF~0.31. The overall efficiency for this solar cell is 1.11 %.

When thermal annealing is applied to the reference device at 140 °C for 2 min (dashed line) the V_{oc} rises up to 0.62 V and J_{sc} increases to 6.95 mA/cm^2. The fill factor for this cell has a value of 0.36. Therefore the efficiency under white light illumination is 1.57 %.

Among the solar cells that have been annealed (at 140°C for 2min) and simultaneously treated by an external electric field, best performance were given by the one with applied voltage equal to 8 V for a duration of 2 minutes. The current-voltage characteristic for this device is represented by the curve with the filled triangles in Figure 1. Electrical characteristic of this cell under illumination with white light are: V_{oc}~0.66 V; J_{sc}~6.79 mA/cm^2; FF~0.50; and overall efficiency of 2.24 %.

Above 8 V we obtained a degradation of performances. Greater bias and longer annealing time degraded the photovoltaic parameters.

The increase of open-circuit voltage (from 0.58 to 0.66) and consequently of the fill factor (from 0.31 to 0.50) of the postproduction-treated solar cells has been explained as a phenomena of burning of shunts [9]. Moreover, the increase in the short-circuit current suggested an enhancement of the mobility of the charge carriers inside the photoactive layer.

Indeed, this production process should facilitate an enhanced crystallization of the polymer annealed at a temperature higher than its glass transition temperature [17]. The additional effect of the

simultaneously applied external voltage should be to support the orientation of the polymer chains in the direction of the applied potential difference, due to the injection of additional charges into the polymer bulk [9,18].

Table 5.1 Photovoltaic parameters of P3HT-PCBM devices annealed at 140 °C for 2 and 10 minutes under various external electric field.

External electric field (V)	time(min)	J_{sc} (mA/cm^2)	V_{oc}(V)	FF	IPCE (%)
0	2	6,95	0,62	0,36	1,57
	10	5,81	0,58	0,31	1,06
2	2	7,18	0,63	0,40	1,82
	10	6,07	0,62	0,36	1,35
5	2	7,15	0,64	0,46	2,10
	10	5,98	0,64	0,41	1,56
8	2	6,79	0,66	0,50	2,24
	10	6,21	0,68	0,43	1,82
12	2	4,96	0,69	0,37	1,25

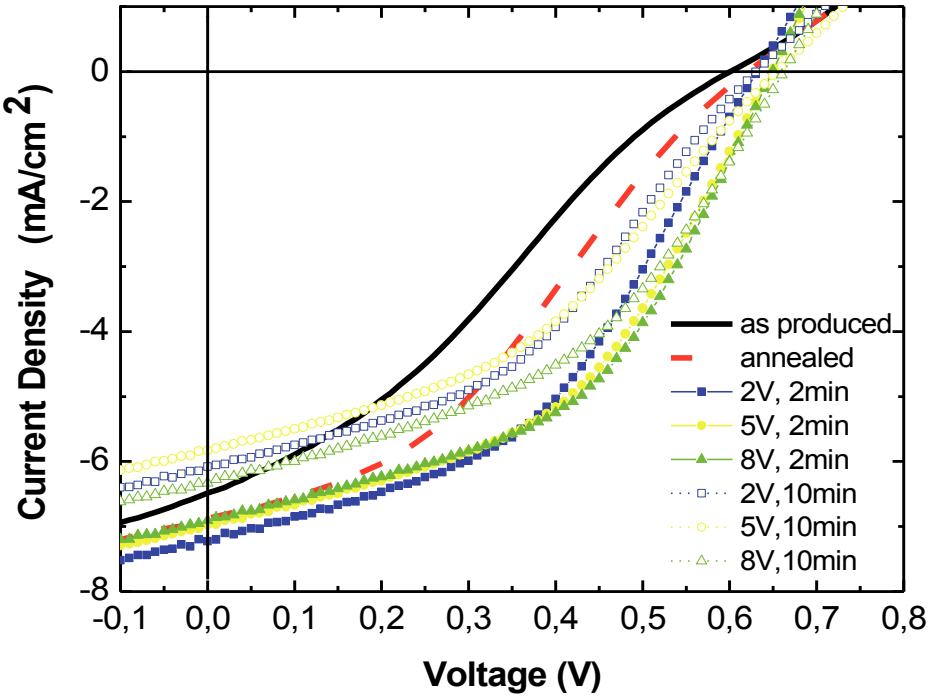

Figure 5.4.1. Current-voltage (J-V) curves of P3HT:PCBM solar cells under illumination with white light at an irradiation intensity of 100 mW/cm^2; as-produced solar cells (straight line), annealed at 140°C for 2 min (dash line), other curves present characteristics of devices annealed at 140 °C for 2 and 10 min under various external electric field.

The results of this study is confirmed by the AFM analysis of the topography the active layer film. Figure 4.3.1 present the morphology of the P3HT-PCBM treated with an annealing temperature of 140'C for 2 min with different values of the applied electric field (a) 2, (b) 5 and (c) 8V. We observe different formation of the morphology dependent on the applied electric field. Two distinct domains are observed to form. The figure shows how an increase of the voltage level allows the formation of a featured film where the domains of the two materials are interpenetrated. While for smaller value of voltage we can see significant

aggregations, nice interpenetrating network is observed for a value of 8 V. The morphology at 8 V comprises small oblong domains with a surface roughness of 260 nm. On the other hands, the morphology of the film at 2 V shows a higher disorder and a roughness of 360 nm.

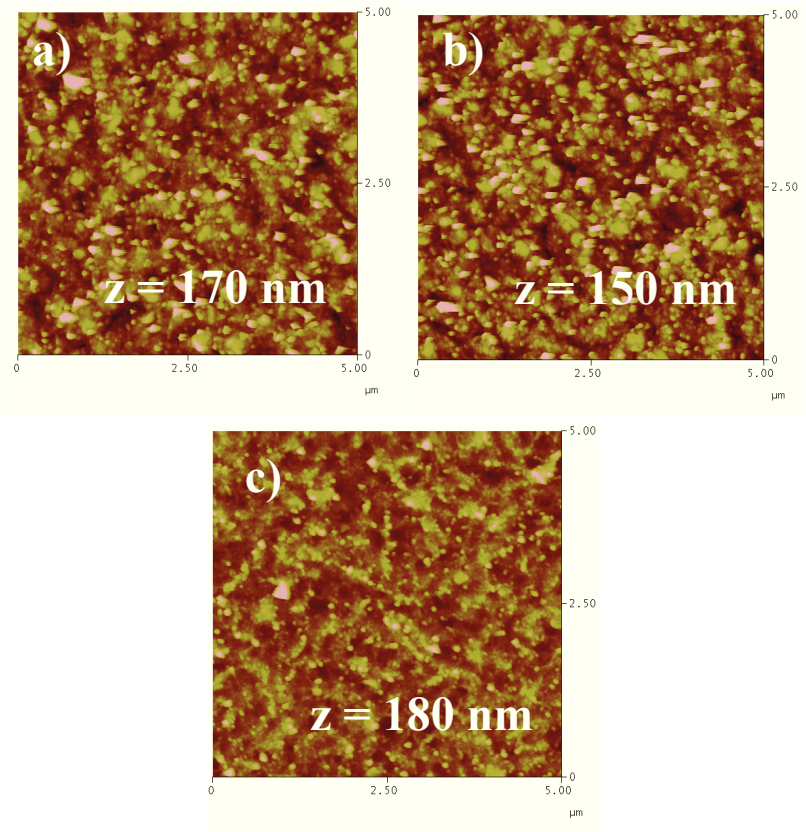

Figure 5.4.2 AFM tapping mode images of P3HT/PCBM film surface after application of an external electric field of value (a) 2 V, (b) 5 V, (c) 8 V and simultaneous annealing on 140 °C for 2min.

Table 5.2 lists the PV parameters for devices exposed to an external electric field without any thermal treatment. Data show that even in the case of no thermal treatment, the performance of the organic solar cells can be improved at the expense of a higher external voltage. In particular, by treating the cells at 12 V for 2 min, we obtained the following results: J_{sc}~7.60 mA/cm^2; Voc~0.59 V; and FF~0.49. The overall efficiency for this solar cell is therefore 2.21 %. Figure 5.4.3 shows the J-V characteristics for devices treated with the applied electric field at 2, 5, 8, 12 and 15 V under illumination with white light.

Table 5.2 Photovoltaic parameters of P3HT-PCBM devices under various external electric field.

Bias (V)	time(min)	J_{sc} (mA/cm^2)	V_{oc} (V)	FF	IPCE (%)
2	2	5,94	0,55	0,29	0,94
5	2	5,76	0,58	0,26	0,89
8	2	6,70	0,58	0,37	1,43
10	2	7,70	0,58	0,40	1,81
12	2	7,60	0,59	0,49	2,21
15	2	5,55	0,58	0,38	1,24

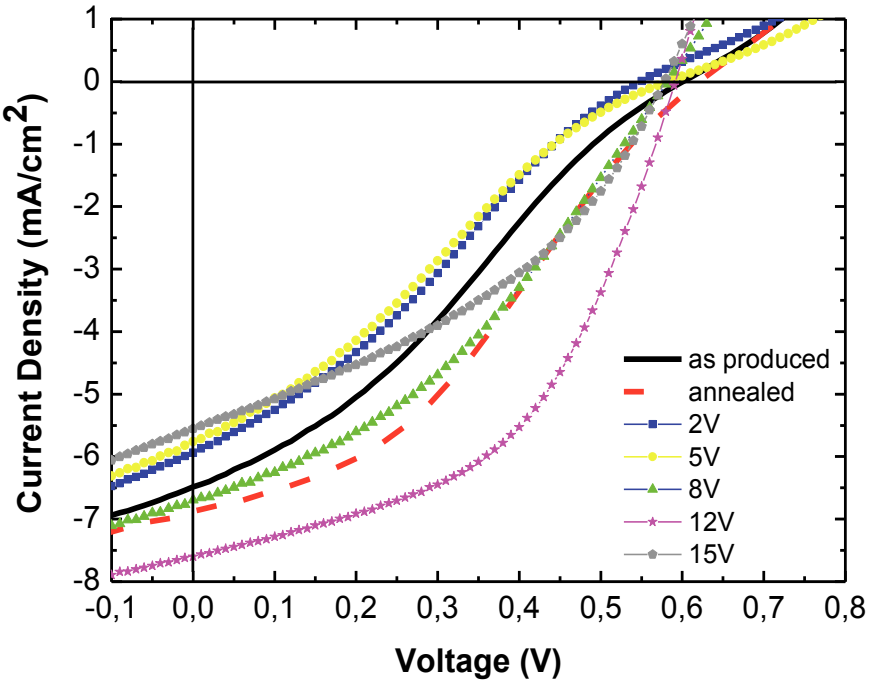

Figure 5.4.3 (color online) Current-voltage (*J-V)* curves of P3HT-PCBM solar cells under illumination with white light at an irradiation intensity of 100 mW/cm^2; as-produced solar cells (straight line), annealed at 140 °C for 2 min (dash line), other curves present characteristics of devices under different external electric field 2, 5, 8, 12 and 15 V for 2 min.

It is interesting as the device treated with 12 V without thermal annealing gives the same FF and similar efficiency as the one treated with 8 V at 140 °C. However, here the difference lays in the fact that the electric treatment has a major effect on the J_{sc} of the device, while the combined treatment, mostly, on the Voc.

Another interesting aspect is that the time at which both treatment give the best result is the same, only 2 minutes. Thus, no long exposure times are needed.

Finally, it can be seen in Figure 5.4.3 as the increase of the external applied electric field potential is beneficial for the cell performances until a point where it degrades (see treatment with 15 V). The same phenomena can be seen in Figure 5.4.1 for devices treated at 12 V.

Table 5.3 Data of the temperature measurements during the characterization of devices with and without additional thermal treatment.

Bias (V)	time (min)	T only with DC (°C)	T with annealing (°C)	current (mA)
2	2	25	153	1,8
	10	25	154	
5	2	27	153	12
	10	28	153	
8	2	30	153	26
	10	31	153	
12	2	37	154	50
	10	40	154	
15	2	46	157	59
	10	50	157	

To better understand the effect of the electric field in isolation we measured the temperature of the devices while treated with and without thermal treatment with thermal camera. Table 5.3 shows the data of this experiment. The temperature of devices treated with thermal treatment of 140 °C for 2 min and external voltage of 8 V is about ~155 °C, while the one of devices without heating treatments with applied external voltage

of 12 V is only around ~37 °C. This suggest that high temperature as a post production treatments is not necessary to obtain highly performing solar cells. Experiments suggest that the application of external electric field can be easily used as a post production treatment to fabricate the polymer solar cells at low temperature process.

5.5 Conclusion

In summary, the effect of annealing under external voltage on the PV characteristics of P3HT/PCBM encapsulated devices and influence of external voltage without thermal treatment have been investigated.

An applied external electric field greater than the open-circuit voltage of the device injects additional charges into the polymer bulk and therefore may lead to a modified orientation of the polymer chains inside the photoactive layer along the direction of electric field. The ordered structure induced by the modified orientation of the polymer chains combined with the efficient percolation pathways increases the mobility of charge carriers. So the Jsc and IPCE can be improved significantly.

Our results show that the effect of an applied electric field in isolation (without annealing treatment) is sufficient to obtain efficiencies given by the combined process (electric field and annealing) at the expense of higher applied voltage. However, this methods gives gains in terms of reduction of temperature and complexity of the fabrication process. In our opinion, this method can easily be integrated into large area and low-temperature fabrication process for the future development of flexible polymer solar cells.

References

[1] N. S. Sariciftci et al, *Science* 258, 1474–1476 (**1992**).

[2] G. Yu et al, *Science* 270, 1789–1791 (**1995**).

[3] J. J. Halls, et al., *Nature* 376, 498–500 (**1995**).

[4] J. Kim, et al. *Science* 317, 222–225 (**2007**).

[5] M.Reyes-Reyes et al, *Appl. Phys. Lett*., 87, 8, 083506-1-083506-3, (**2005**).

[6] G. Li, et al. *Nature Mater*. 4, 864–868 (**2005**).

[7] Y.Kim, et al., *Nature Mater*. 5, 197–203 (**2006**).

[8] W. Ma et al, *Adv. Funct. Mater*. 15, 1617–1622 (**2005**).

[9] A.C. Arias et al., *Macromolecules* 34, 6005-6013, (**2001**).

[10] Y.S. Kim et al., *Current Applied Physics* 10, 985-989, (**2010**).

[11] J.A. Renz et a., *Solar Energy Material&Solar Cells* 93, 508-513, (**2009**).

[12] X. Yang, et al., *Nano Lett.*Vol.5, No.4, (**2005**).

[13] D. Chirvase, et al., *Nanotechnology* 15, 1317-1323, (**2004**).

[14] D. Chen, A.Nakahara, D.Wei, D.Nordlund, T.P. Russell, *Nano Lett*., 11, 561-567, (**2011**).

[15] F. Padinger et al, *Adv. Funct. Mater*., 13, 1, (**2003**).

[16] H. Jin et al, *Solid State Commun.* 140, 555-558, (**2006**).

[17] C.C. Lin et al., *Energy Environ. Sci.*, 4, 2134, (**2011**).

[18] A. Bagui, S.S.K. Iyer, *IEE Transaction of Electronic Devices*, 58, 11, (**2011**).

[19] H.Hoppe, et al., *Adv. Funct. Mater*. 14, 1005-1011, (**2004**).

[20] http://www.ossila.com

[21] T. M. Brown et al, 93, 6159 (**2003**).

[22] T. M. Brown et al. 12, 623 (**2011**).

[23] Y. Li et al, *Synthetic Metals* 158, 190–193,(**2008**).

[24] H. Jin et al *Solid State Commun*. 142 , 181 (**2007**).

6 Stability and degradation

6.1 Introduction

In last few years, research in the field of polymer and organic solar cells have experienced a rapid progress and big improvement. However, in terms of research trends, the main direction has been towards the achievement of a high power conversion efficiency under simulated sunlight. Efficiency of OSCs has been increased up to 10.7% [1], but for successful commercialization of OSCs, and in order to compete with the more mature silicon technology, where the lifetime is approximately 25 years, such products should not only offer high efficiency but factors like *process* and *stability* should be taken into consideration (figure 6.1.1).

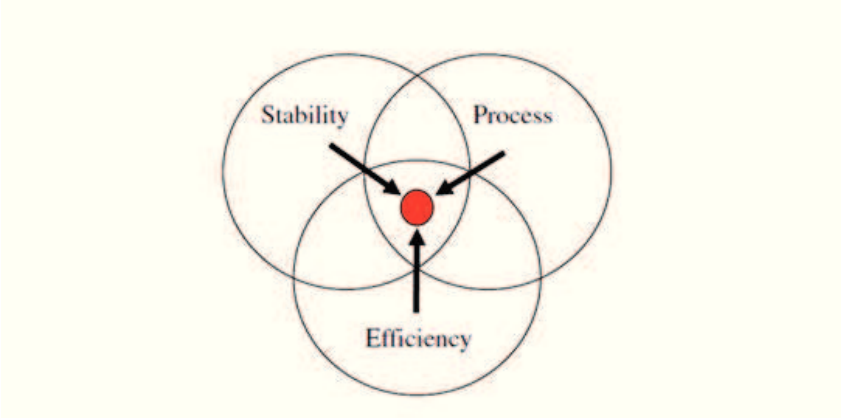

Figure 6.1.1. The challenge of unifying efficiency, stability and process for the same material [2].

Until the research is focus on just one of these areas, progress towards application of the technology are likely to be slow as breakthrough in one of the area is very unlikely to automatically render solutions in the other two areas. Relatively little consideration has been given to these individual areas, especially, to the poor device stability of organic solar cells which are more liable to chemical degradation from, e.g., oxygen and water, than inorganic materials.

6.2 Historical overview and background

A number of studies have been carried out and they show that the stability/degradation issue is rather complicated and certainly not yet fully understood. The graphical summary of studies on stability of OPVs from the last few years is shown on figure 6.2.1

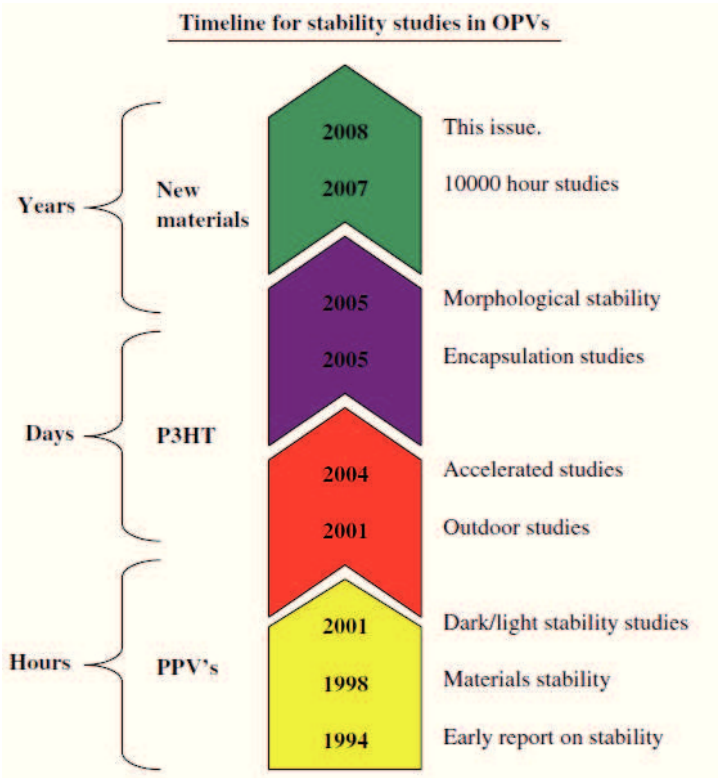

Figure 6.2.1. A graphical overview of the field of stability and degradation of polymer solar cells. The lifetime under atmospheric conditions and the typical materials is estimated on the left-hand side [2].

In the early 1990s organic solar cells had operational lifetimes of hours or days. Clearly, improvements have been made as confirmed by a recent study by Krebs and Norrman [3], where it has been reported OPV life-times of up to 10,000 hours. In 2008, another study, carried out by Hauch et al. [4] reported a cell tested outdoors with a lifetime of more than one year.

Degradation is mainly a consequence of the effect of the **diffusion of oxygen and water** into OPVs when tested in ambient air [5]. The

diffusion of these molecules into the cell was tracked and quantified by Norrman et al. [6], who developed a way to isotopically label oxygen or water. Studies [7] showed that:

- oxygen enters through the back electrode through microscopic pinholes in the electrodes surface;
- exposition to light of the cell has no influence on the diffusion of oxygen and water; and
- exposition to light has a negative effect on oxidation of the layer immediately below the electrode.

Degradation can be related also to **electrochemical reactions taking place at the electrodes**. Aluminum, a common material used in normal geometries, is a metal that reacts with oxygen and water. The result is the formation of an insulating oxide layer between the active material and the aluminum electrode [8].

Jong et al. [9] studied **the stability of the interface between indium–tin oxide and PEDOT:PSS**. They summarized that the ITO/PEDOT interface is very sensitive to air. The hygroscopic nature of PSS allows absorption of water which facilitate etching of the ITO layer which was confirmed by a group of Kawano et al. [10,11].

Approaches used to minimize the effects of diffusion that have been proposed are:

- encapsulation can make a cell retain over 80% of its original PCE after 40 days under ambient conditions (see Hau et al. [12] on unencapsulated, inverted P3HT:PCBM cells).
- In the same study was shown that conventional cell, by contrast, lasted only four days.
- The aluminum electrode can be replaced with a less reactive, high work function metal, e.g., silver or gold [13].

- A buffer layer more stable than the PEDOT layer (e.g., ZnO or TiOx nanoparticles) can be spin coated or printed on top of the ITO electrode in inverted cells [14].

Degradation mechanism is not yet completely understood, but it is clear that organic photovoltaic devices are sensitive to oxygen and water and it is necessary to develop effective and stable encapsulation method to protect the fragile morphology of the active layer. Research has been carried out to find the encapsulation requirements for organic devices. At the state of the art in the fabrication of encapsulated devices:

- the transparent substrate is made of glass, which is impermeable;
- the thin metal electrode is porous, giving problems if gas absorption;
- the flexible substrates show fast transport of oxygen and water.

The encapsulation used by Krebs [15], which allowed more than 1-year operation of a large area P3HT/PCBM bulk heterojunction, is probably almost totally impermeable to both oxygen and moisture due to the rigid technique that has been used (where the device is sandwiched between a thick aluminum back plate and a front glass plate).

In this section we present degradation studies of devices based on P3HT-PCBM bulk heterojunction encapsulated by a transparent glass substrate that is stuck on the device by epoxy glue. We investigated the performance evolution over a period of 96 days in ambient conditions.

6.3 Device preparation

Devices were fabricated as described in Section 5.2.

6.4 Characterization

All devices were illuminated through ITO electrodes through the glass cover slip. Current-voltage (J-V) measurements were carried out by a Keithley 2400 source unit and our prototype board (with allowed electrical connection to the six individual pixels), under AM1.5 solar simulator with illumination of 100 mW/cm^2. Between the measurements devices were kept in the ambient conditions in the dark.

6.5 Results and discussion

The current density–voltage (J–V) measurements of an encapsulated device based P3HT-PCBM at various intervals of time during the 96 days after their fabrication are shown in Fig.6.5.1. The figure shows a continuous degradation of all photovoltaic parameters.

Experiments (table 6.1 and Figure 6.5.2) show the following results:

- Jsc degraded form its initial value of 6.48 to 6.16 mA/cm^2 during the first 46 days (5 % degradation) and up to the amount of 4.92 mA/cm^2 after 96 days, which gives the degradation of 24 %.
- Open circuit voltage remained quite stable during the period of 3 moths measurements, degradation of only 4% from starting value of 0.56 up to 0.54 V.
- Fill factor decrease from 0.35 to 0.27 after 96 days.

Finally, efficiency decrease from the initial value of 1.28 % throughout the 3 months period, mainly due to the degradation of Jsc, to the value of 0.71 %. This gives degradation of the efficiency of 45 % after the period of 3 months.

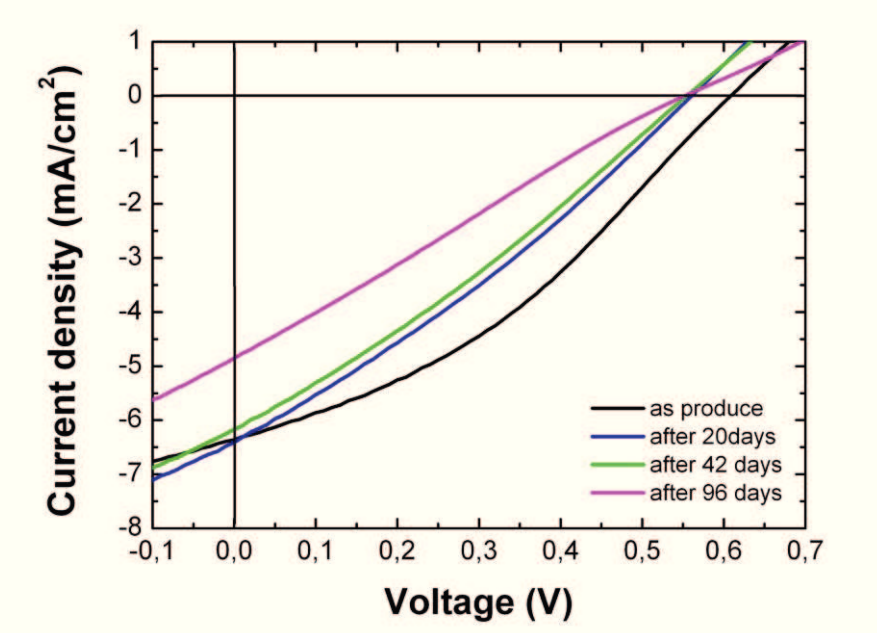

Figure 6.5.1. Current-voltage (J-V) curves of degradation of encapsulated devices based on P3HT:PCBM solar cells under illumination with white light at an irradiation intensity of 100 mW/cm^2, black line – as produce, blue line – degradation after 20days, green line – after 42 days, pink line- after 96 days.

Table 6.1. Evolution of performance of encapsulated devices based on P3HT-PCBM obtain from J-V characteristics (under an illumination of 100 mW/cm2 with an AM 1.5 G solar simulator).

	as produced	20 day	42 days	96 days
Jsc (mA/cm^2)	6,48	6,35	6,16	4,92
Voc (V)	0,56	0,55	0,54	0,54
FF	0,35	0,33	0,32	0,27
IPCE (%)	1,28	1,17	1,08	0,71

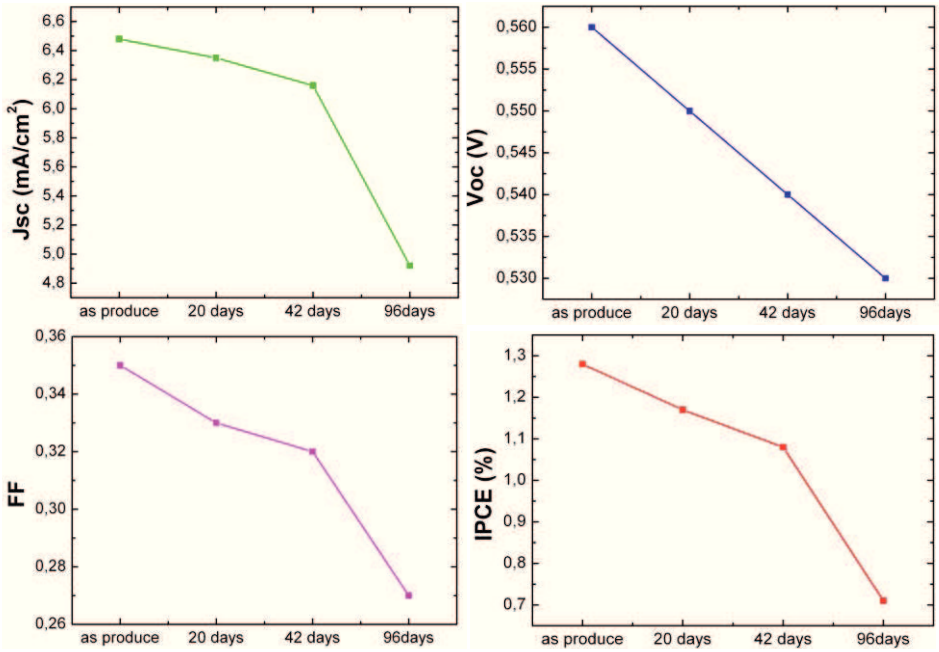

Figure 6.5.2 Evolution of the averaged performance parameters of encapsulated organic solar cells.

It was found that oxygen and moisture diffusion through the outer electrode (counter electrode to ITO) [16] is the most important factor responsible for degradation of organic solar cells. Diffusion proceeds via grain boundaries and microscopic pinholes in the metal electrode (cathode) depend on the electrode morphology, i.e. grain size distribution, hole sizes, hole density.

The reaction of P3HT with oxygen has not been investigated yet. However it is known, that P3HT form charge transfer complexes with oxygen shown in Fig. 6.5.3 [17].

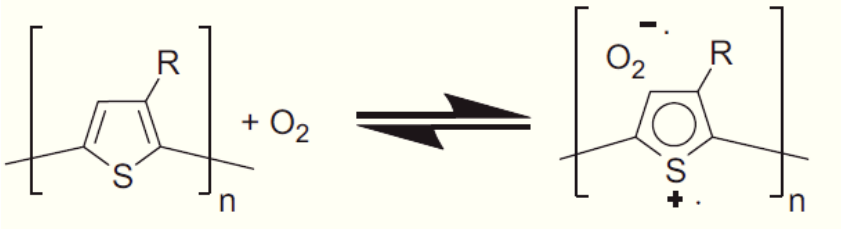

Figure 6.5.3. Reversible formation of a charge transfer complex between P3AT (A=alkyl) and oxygen. R represents an alkyl group [17].

The formation of charge transfer complexes between oxygen and P3HT is reversible but does not in itself lead to degradation of the polymer. Photosensitization of singlet oxygen by triplet states on P3HT seems unlikely due to the very low triplet quantum yield of this polymer. Singlet oxygen may be formed on dissociation of the excited state of the charge transfer complex. Thiophenes react with oxygen at low temperature under irradiation to form thioozonides, which undergo further degradation at room temperature as shown in Fig. 6.5.4 [18].

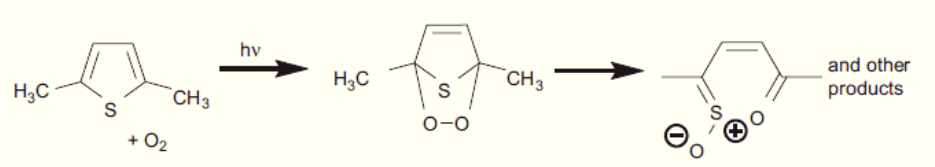

Figure 6.5.4. Reaction between 2,5- dimethylthiophene and oxygen initially forming a thio-ozonide intermediate that can then decompose to an S-oxide and other products.

A slower reversible component that depends on the light intensity occurs at the time-scale of minutes. Matturro et al.[18] suggest that the slow reaction involves metastable oxygen species that are later responsible for the irreversible degradation of the polymer.

6.6 Conclusions

One of the greatest obstacles that must be overcome is the inability to produce stable solar cells with long lifetimes. As detailed above, some progress has been made. But organic solar cells are complicated multilayer structures where each component may fail for different reasons and layers may even interact chemically and physically in ways that may cause degradation. Oxygen from the atmosphere will oxidize the organic layer. Fortunately, newer materials like P3HT are less prone to this degradation. Most organic solar cells today rely on the formation of bulk heterojunction. The phase-separation morphology, developed through the process of annealing is very important to obtain efficient devices. But this structure is not at the thermodynamic equilibrium, so further structural changes can occur, especially when devices are heated. More stable devices have already been made and progress in this research field is important for polymer solar cells to have a future as commercial devices.

Fabrication in glove boxes followed by immediate encapsulation is a common laboratory technique used to maximize device lifetimes and improve stability. Unfortunately, large-scale production of OPVs in inert environments is not feasible. In order to keep down costs, ambient processing of organic solar cells is essential.

New techniques need to be investigated to let organic solar cells compete with silicon technology and high customer request for efficient and long lifetime solar cells.

References

[1] http://www.heliatek.com

[2] M. Jørgensen et al., *Solar Energy Materials & Solar Cells*, **2008**, 92, 686–714

[3] F. C. Krebs, *Progress in Photovoltaics:Research and Applications*, **2007**, 15(8):697.

[4] J. A. Hauch et al., *Solar Energy Materials and Solar Cells*, **2008**, 92(7), 727-731,.

[5] M. Jorgensen et al., *Solar Energy Materials and Solar Cells*, **2008**, 92(7), 686-714.

[6] K. Norrman, F.C. Krebs, *Surface and Interface Analysis*, **2004**, 36(12), 1542-1549.

[7] K. Norrman et al, *Solar Energy Materials and Solar Cells*, **2006**, 90(17), 2793-2814.

[8] M. Glattharret al., Solar *Energy Materials and Solar Cells*, **2007**, 91(5), 390-393.

[9] M.P. de Jong et al, *Appl. Phys. Lett.,* **2000**, 77 2255.

[10] R. Pacios et al, *Adv. Funct. Mater,* **2006**, 16, 2117.

[11] K. Kawano et al, *Sol. Energy Mater. Sol. Cells*, **2006**, 90, 3520.

[12] S. K. Hau at al., *Applied Physics Letters*, **2008,** 92(25):253301-253301(3).

[13] M. Tavakkoli et al., Solar *Energy Materials & Solar Cells,* **2011**, 95 1964–1969.

[14] F. C. Krebs., *DEStech Publications, Inc*., Lancaster, Pennsylvania, **2010**.

[15] F.C. Krebs, *Sol. Energy Mater. Sol. Cells,* **2006**, 90, 3633.

[16] K. Norrman et al, *Sol. Energy Mater. Sol. Cells,* **2006**, 90, 2793–2814.

[17] M.P. de Jong, *Appl. Phys. Lett*., **2000**, 77, 2255–2257.

[18] M.G. Matturro et al, J. Am. Chem. Soc., **1986**, 108 2775.

7 Small band gap molecules HBTP-PCBM blends

7.1 Introduction

Research on bulk-heterojunction organic solar cells has, mainly, focused on polymeric donor materials [1]. This can be attributed to better film-forming characteristics and film morphology of polymers, than their small-molecule counterparts.

To achieve a high efficiency, solar cells need to absorb as much light as possible. This requires a good match between the absorption of the active polymer and solar spectrum in photon flux [2]. The photon flux regime in solar spectrum has its maximum around 700 nm. Although a PCE of 2-6% has been achieved [3,4], the widely used P3HT:PCBM

system has been limited in further improvement. This is because of a weak absorption of polymers above 650 nm.

Ideal conditions for the solar cells are that every absorbed photon can be convert into an electron. The maximum theoretical current density is 14.3 mA/cm^2 in a system that could absorb light up to 650 nm, 17.6 mA/cm2 for 700 nm and 23.9 mA/cm2 for 800 nm, as shown in. It is becoming critical to expand the absorption region beyond 650 nm, i,e., to develop low band gap polymer materials. To obtain low gap polymers, there are three main strategies: lowering the LUMO level; increasing the HOMO level; in both ways. Voc would suffer a decrease if we bear in mind that it is related to the offset between the HOMO of a donor and the LUMO of an acceptor. On the other hand, the reduction of LUMO(D)-LUMO(A) offset will be destruct of electron transfer if this offset is lower than exciton bonding energy, typical larger than 0.3 eV [5,6]. In this respect, it is crucial as well to find or develop acceptor materials to match the LUMO of donors.

But polymers pose several. A possible solution to these problems could consist in the replacement of π-conjugated polymers by soluble small conjugated molecules as donor material. Such an approach would present several potential advantages:

1. A perfectly defined chemical structure erases the problems posed by the structural variability of polymers, namely, the control of the regioregularity, molecular weight, and polydispersity,as well as the elimination of remnant bromide groups.
2. Purification of a single molecule is in general easier than that of a polymer.
3. Materials derived from molecular elemental units show in general higher charge-carrier mobilities than polymers.

4. The analysis of the relationships between chemical structure, electronic properties, and device performances is more straightforward than that for polymers for which structural modifications can indirectly affect the electronic properties through changes in molecular weight, polydispersity, and effective conjugation length.
5. The high molecular extinction coefficients of many molecular dyes permits limiting the thickness of the active layer, thus minimizing problems associated with charge transport and series resistance.
6. Many small dye molecular structures can be viewed as quasi-spherical particles, which can be more appropriate to isotropic optical and transport properties than linearly conjugated systems [7,8].

Research on small molecule solar cells started in 1986 and, since then, a large number of studies have used small molecules for organic solar cells [9-15]. These studies have highlighted that, although small-molecule donor materials can also form useable BHJ solar cells by solution processing but it is more challenging to obtain high-quality films. Solar cells made of small molecules reach about 4% of efficiency [16], yet these are all laboratory values. In terms of efficiency, small-molecule solar cells are currently lagging behind polymer-based solar cells. There are three possible reasons.

- The materials base for polymers has improved considerably in recent years, much more than for small molecules.
- Comparing standard polymers with small molecules used for organic solar cells, currently higher charge carrier mobility is obtained in polymers [17-19].

- Finally, there are more known ways of controlling the morphology, for example by choice of solvents [20,21], annealing temperature [22-25], and concentrations of ingredients in the absorber solution [26].

The term BHJ is often used to refer to a bicontinuous, interpenetrating network of donor and acceptor phases; however, when two low-molecular weight solids are deposited from solution in a manner similar to polymer BHJs, the two materials may not form bicontiuously or interpenetrating as observed in polymer counterparts. Nonetheless, they may still produce a photovoltaic effect [27]. As a general trend with most of the SMBHJ materials, the Voc tends to be higher than that observed in analogous polymer devices, while the FF and Jsc of SMBHJs are usually considerably lower. Examining the light versus dark curves for most of the devices shows that in almost all cases, the photocurrent produced by SMBHJs becomes significantly larger at reverse bias. These points seem to imply that carrier extraction and recombination limit current generation in these SMBHJs much more than is the case in polymer based BHJs. This trend could be explained in terms of the morphology of molecular heterojunctions, where small molecules tend to result in morphologies with more

- *charge-trapping "cul-de-sacs"* and
- *dead ends*,

whereas higher-molecular-weight polymers more readily form percolated networks with continuous carrier transport pathways to electrodes [28]. Unfortunately, this hypothesis is difficult to verify directly because of the difficulty and limitation of characterization methods to analyze the cross-sectional composition of such films.

The next big challenge in SMBHJs may be finding strategies to control the morphology to maximize D-A interfacial area while

minimizing structurally induced recombination losses; allowing for large short circuit currents and high fill factors in SMBHJ. The ability to fine-tune the phase separation and self-assembly of molecular solids via synthetic design may put them in a position to compete with polymers as the preferred type of organic semiconductor for high efficiency solar cells [29].

In this chapter we present the photovoltaic properties of a new material called HBTP-db-118 incorporated with PCBM.

7.2 HBTP-db-118

We investigated a new small molecule from the University of Wuppertal in Germany called HBTP-db-118 5,7-Bis-(5'-hexyl-[2,2']bithiophenyl-5-yl)-2,3-dimethyl-thieno[3,4-b]pyrazine.The structure of HBTP is shown in Figure 7.2.1.

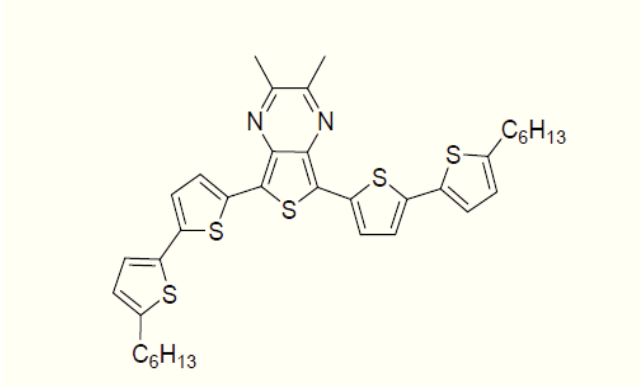

Figure 7.2.1. Chemical structure of HBTP-db-118.

The energy level of the highest occupied molecular orbital (HOMO) was determined by cyclic voltammetry (CV) measurements. This was conducted by Dima in the labs of Dr. Daren Caruana (UCL-Chemistry). The energy level of the lowest unoccupied molecular orbital (LUMO) was calculated using the energy gap calculated from the corresponding UV/Vis spectra of the IR-polymers in solution. The data for P3HT & PCBM in Figure 7.2.2 have been taken from the literature [30].

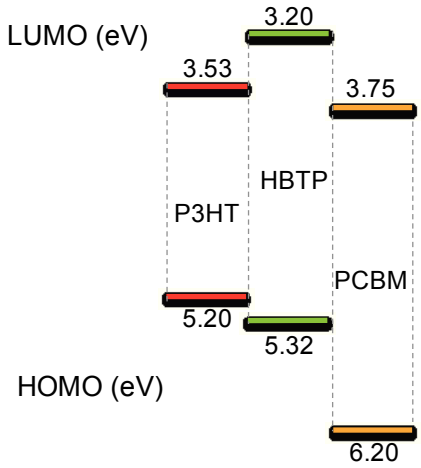

Figure 7.2.2. Energy levels of the materials used in the experiments (HBTP,PCBM).

HBTP has been synthesized to have a small difference between HOMO and LUMO levels.

The HBTP energy levels are close to P3HT. This suggested us to investigate it as an electron donor with PCBM as electron donor for photovoltaic devices.

In figure 7.2.3 can be seen the absorption and photoluminescence of the molecule in solution of dichloromethane (data from Wuppertal). Further data from Wuppertal are summarized in Table 7.1. The emission spectrum reveals a single Gaussian shaped peak emission at 723 nm, which corresponds to a band gap of 1.71 eV. Absorption shows strong features with distinct Gaussian peaks at 273, 390 and 571 nm (due to transitions of 4.53, 3.17, and 2.16 eV, respectively).

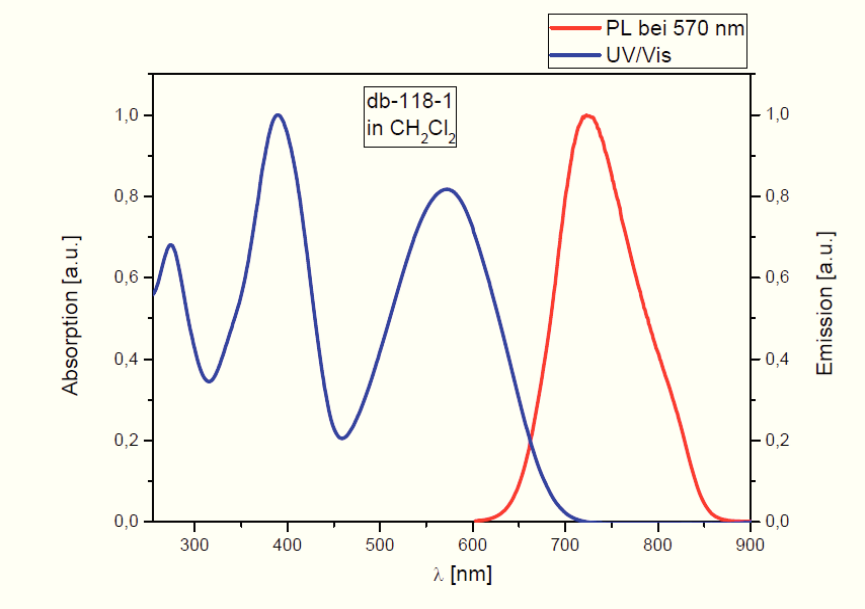

Figure 7.2.3. Absorption , photoluminescence spectra of HBTP. This data was obtained in Wuppertal**.**

Table 7.1. Optical properties of the HBTP molecule from solution in CH_2CL_2 (data from Wuppertal).

	Absorption peak positions (nm)	PL peak position (nm)	M_n (g/mol)
HBTP	273 (0,68) 390 (1,00) 571 (0,82)	723	350

There is very little spectral overlap between emission and absorption. The HOMO/LUMO values of 5.32 and 3.20 eV represent average values of statistical distributions of HOMO/LUMO levels. The range of energy gaps apparent in the absorption and emission spectra demonstrates that there are several available energy transitions in HBTP. The heavily red-shifted emission indicates that HBTP effectively transfers energy to, and emits from, its lowest energy states. Energy migration from higher to lower states is common for conjugated materials The PL emission of HBTP in dichloromethane peaks in the deep red part of the spectrum, but extends past the near infrared. This means that HBTP shows potential as an NIR emitter.

7.3 Solution preparation

HBTP and PCBM were dissolved in chlorobenzene separately, with a concentration of 22 mg/ml each (2% wt) and then stirred in air and heated at temperature of ~70° over night. HBTP dissolved poorly in chlorobenzene and even under high temperature (~100°) the solution quality was still poor with many particles not dissolved. Solutions were then filtered (0.45μm) and mixed together in different ratios: HBTP:PCBM = (20%/80%), (30%/70%), (40%/60%), (50%/50%),

(55%/45%), (60%/40%), (70%/30%), (80%/20%), Successively, the solution was stirred and gently heated for several hours.

A non-filtered solution with ratio 1:1 was also prepared.

7.4 Device preparation

Small molecules bulk heterojunction (SMBHJ) solar cells were produced in the following structure: ITO / PEDOT:PSS (~100 nm) / active layer (~120 nm) / Al (150 nm) (Figure 7.4.1).

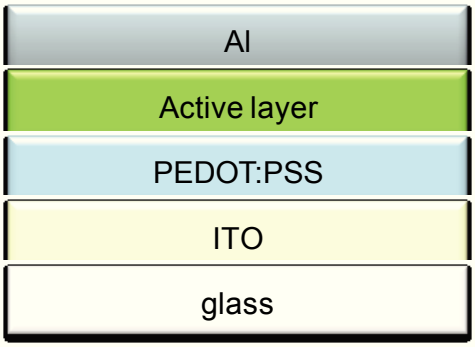

Figure 7.4.1. Schematic structure of the device.

Indium tin oxide (ITO) substrates were ultrasonically cleaned with acetone and isopropanol for 15 min each before being subjected to the O_2 plasma treatment for 15 min.

PEDOT:PSS poly(3,4 ethylendioxythiophene)-poly(styrenesulfonate) was filtered (0.45 μm) and then spin-coated in air on the top of the clean ITO substrates immediately after the O_2 plasma treatment at a speed of 4000 rpm for 60 s. The resulting thickness of the layer was about 100 nm.

After backing the PEDOT:PSS for 15 min at 140 °C on a hot-plate inside the nitrogen glove-box a thin layer of the HBTP/PCBM solution was spin-coated on the top-surface at different speed 700 rpm, 800 rpm, 900 rpm, 1000 rpm, 1100 rpm. The resulting thickness range was between 80 and 130 nm.

Finally, aluminium electrodes were thermally evaporated on top of the organic active layer under high vacuum conditions at an evaporation rate of 2 Å/s forming a layer of the aluminium of 150 nm. The base pressure during the evaporation was $4*10^{-6}$ mBar. About 0,8 kA of aluminium was pre-evaporate before the proper evaporation.

The devices were completed by thermal annealing on a hot plate at different temperatures and different time (5min 50°, 5min 100°, 5min 180 °C, 15 min 150 °C, 1 h 100 °C) inside the nitrogen-filled glove box. Non-annealed control devices were also tested.

7.5 Characterization

Devices with an active area of 14 mm^2 were characterized by current-voltage (J-V) measurements in vacuum by using a Keithley 2400 source unit under AM1.5 conditions with illumination of 100 mW/cm^2.

The incident-photon-to-converted-current efficiency (IPCE) was measured with the help of solar simulator Sun 3000 110*110 mm, Abet Technologies.

Thicknesses were measured using a Dektak surface profilometer.

All atomic force microscopy (AFM) images have been recorded in tapping mode using a Veeco Instruments NanoScope Dimension 3100.

7.6 Results and discussion

7.6.1. Absorption and thickness

In Figure 7.6.1.1 we report the device absorption spectra (not-corrected for reflectivity) for different HBTP:PCBM concentrations. Greater absorbance is obtained in case of higher presence of HBTP, and around intermediate ratios. However, several absorption spectra display a low-energy tail extending to 700-800 nm which is suggestive of significant scattering, and of a rough morphology that is also confirmed by AFM investigations, as reported in section 7.6.4.

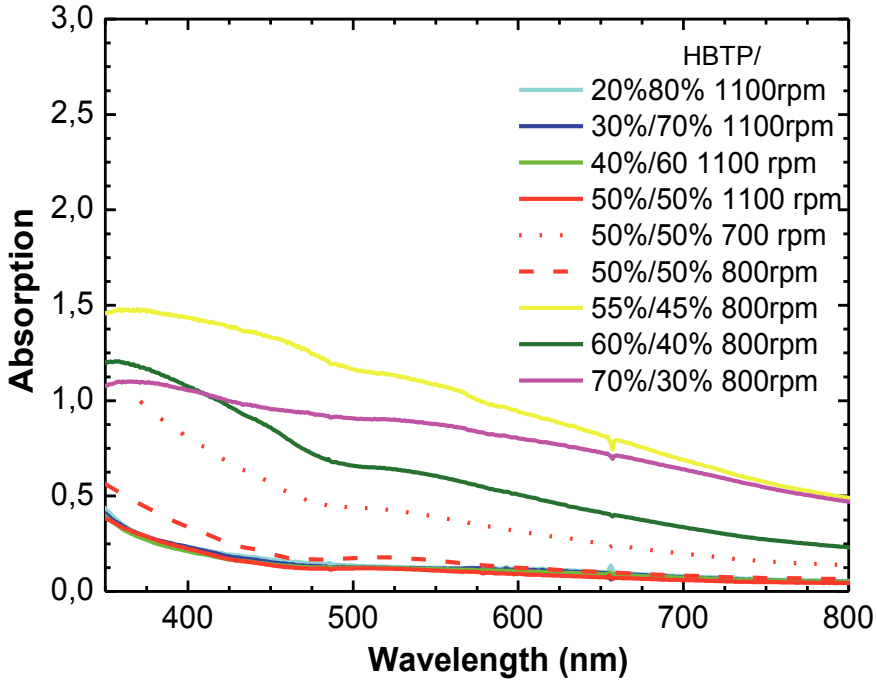

Figure 7.6.1.1. Normalized UV-visible absorption spectra of HBTP/PCBM in films state for different ratios and film thicknesses.

7.6.2. J-V curve characteristic

Figure 7.6.2.1 shows the J-V characteristics of HBTP/PCBM devices for different weight ratios. All active layers were annealed for 5 minutes at 100 °C under nitrogen.

The HBTP:PCBM = 20 %:80 % device shows the best performance with a V_{oc} of 0.161 V, short–circuit current (J_{sc}) of 0.415 mA/cm^2, and fill factor (FF) of 0.30 and PCE of 0.021 %.

Higher concentrations of the HBTP: 80 %, 70 %, 40 % results in very low J_{sc} of less than 0.1 mA/cm^2, V_{oc} of less than 0.1 V and FF of about 0.20. This may be due to very rough and non-uniform structure of the film that scatters the light instead of absorbing. The photovoltaic characteristics for different blend ratios and annealing temperatures are summarized in Table 7.2.

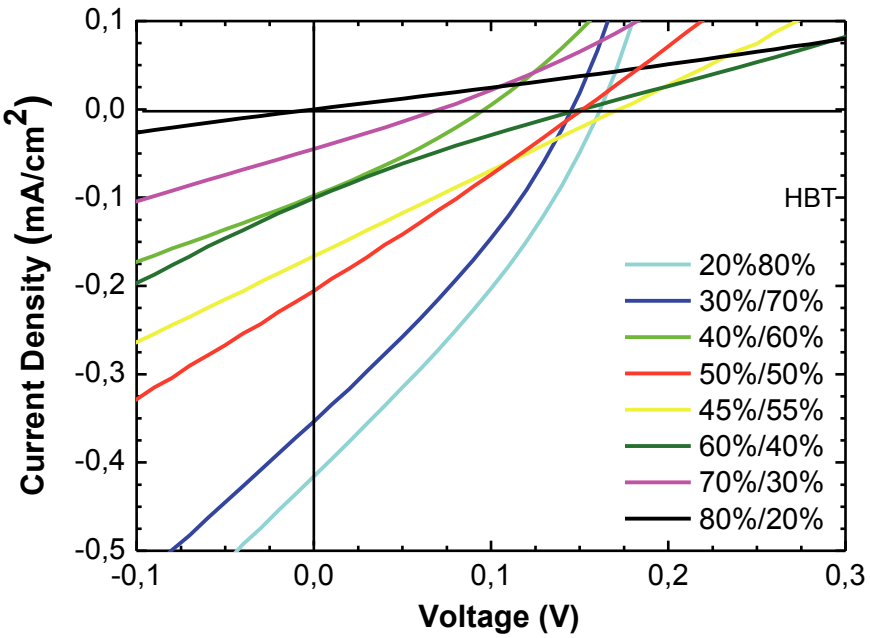

Figure 7.6.2.1. J-V characteristics of HBTP:PCBM devices under AM 1.5 illumination of 100 mW/cm^2 for different ratios. Filtered solution. Post annealing data: 5 min, 100°C.

Table 7.2. A summary of the principle properties of the devices.

HBTP/PCBM filtered, post annealing 5min 100°	**J_{sc} (mA/cm^2)**	**V_{oc} (V)**	**FF**	**PCE(%)**	**Thickenss layer (nm)**
20%/80%	0,415	0,162	0,305	0,021	60±8,7
30%/70%	0,354	0,146	0,301	0,016	80±9,2
40%/60%	0,098	0,097	0,286	0,003	105±24
50%/50%	0,206	0,152	0,262	0,009	128±29
55%/45%	0,166	0,173	0,249	0,007	195±40
60%/40%	0,101	0,151	0,222	0,003	180±22
70%/30%	0,044	0,071	0,259	0,001	102±20
80%/20%	0,000	0,002	0	0	-
HBTP/PCBM non filtered					
50%/50% post annealing 15min 150°	0,719	0,213	0,304	0,046	180±23
50%/50% post annealing 5min 100°	0,333	0,072	0,265	0,006	180±23

In Figure 7.6.2.2 are reported the J-V characteristics in case of filtered and non-filtered solutions with various post annealing treatments. Surprisingly, non-filtered solutions appear to be much better than the filtered ones. Filtration removes high molecular weight part of the material.

In the case of these four samples we observed that for non–filtered solutions a longer treatment i.e. 15 min with the high temperature of 150° shows the best performance with a V_{oc} of 0.213 V, short–circuit current (J_{sc}) of 0.719 mA/cm^2, and fill factor (FF) of 0.30 and PCE of 0.046%. Instead short treatment of 5min and lower temperature of 100° cause lower performance of the device.

We observed opposite behaviour of the filtered solutions. Shorter treatment of 5min and lower temperature of 100 °C are favourable.

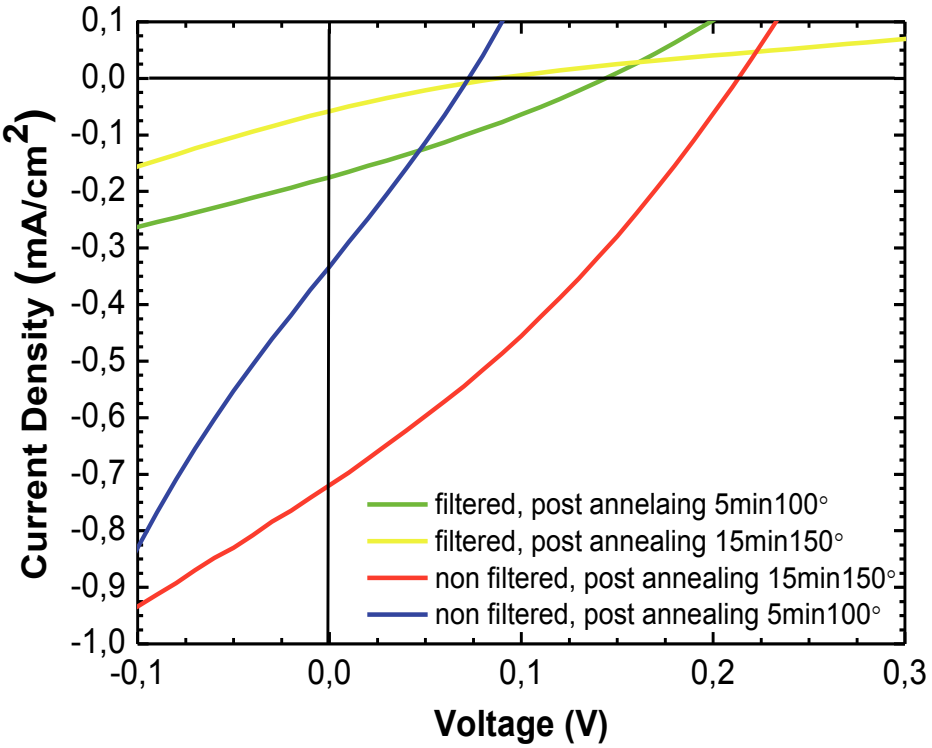

Figure 7.6.2.2. J-V curve characteristic in case of different post annealing treatments and in case of filtered and non-filtered solutions. The ratio of HBTP:PCBM=1:1.

In Figure 7.6.2.3 the effects of the post annealing treatments for filtered solution are shown for a ratio of HBTP:PCBM=1:1. Increasing the time and the temperature of the treatment implies a reduction of the device performances. The optimum annealing treatment is at the temperature of 100 °C for 5 min.

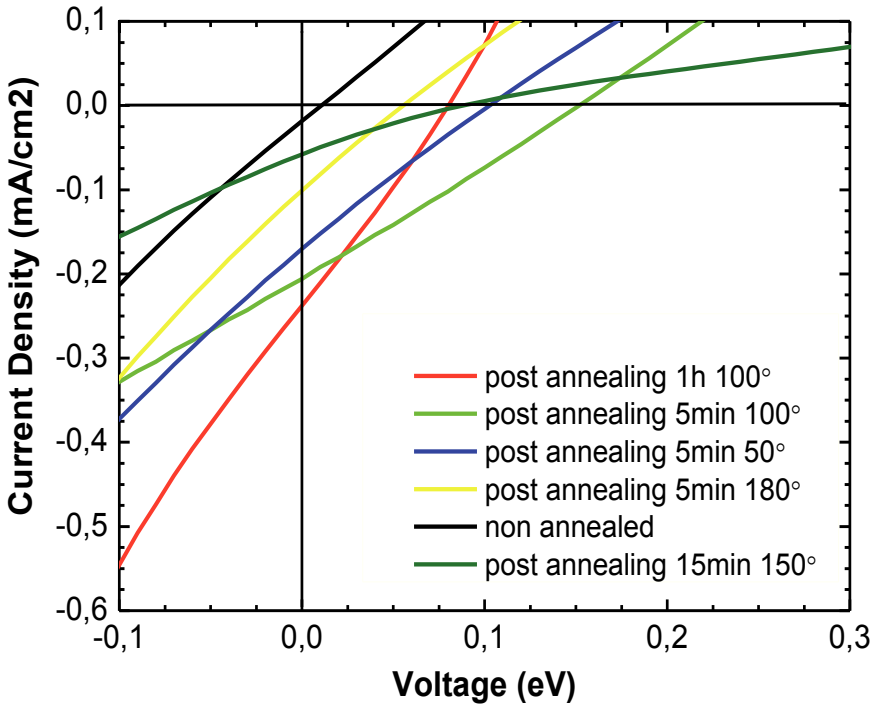

Figure 7.6.2.3. Effect of the post annealing treatment on J-V curve characteristic. The ratio of HBTP:PCBM=1:1

7.6.3. IPCE

In Figure 7.6.3.1 the IPCE of the device is shown for different ratio of HBTP:PCBM. From the graph is not possible to extract a trend that can be used as an indicator of the effect of concentration on the IPCE. In fact, better performance are obtained for a concentration of HBTP 55 % and 30 %, while intermediate concentration levels show worst performances. Very high and very low percentage of HBTP are to be avoided while intermediate level seem to result in a better efficiency.

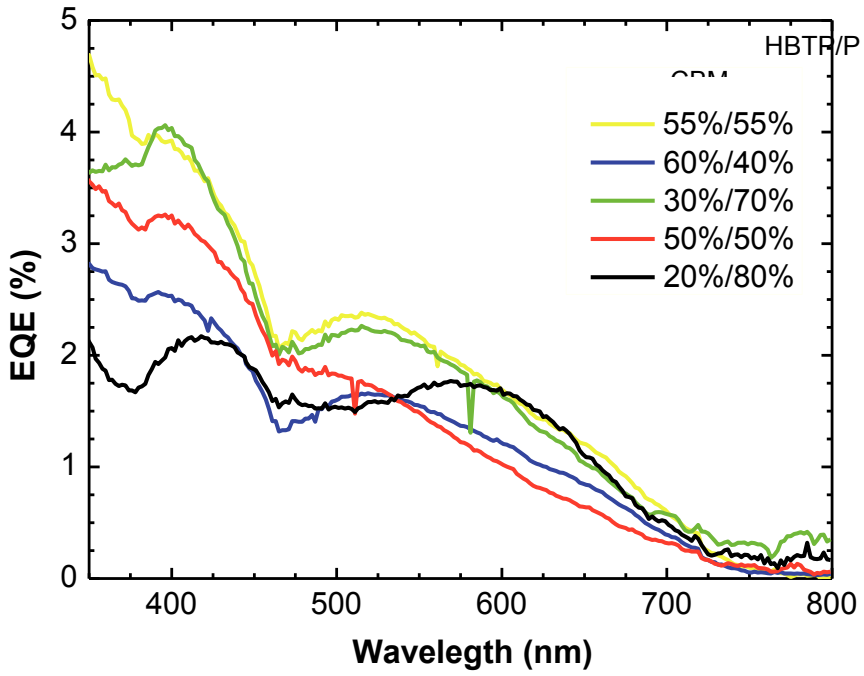

Figure 7.6.3.1. IPCE curves of HBTP/PCBM devices with different ratios. Post annealing data: 5 min, 100 °C.

7.6.4. AFM Images

In Figure 7.6.4.1 AFM images of the film for 2 different ratio are shown. Isolated fibres of HBTP are present. It was not possible to take images at increasing ratios of HBTP because of the increasing height roughness of the film. We can see that there is big difference of the nanostructure obtain for different ratios. Non filtered layers shown on figure e and f seemed to be more density packed and concentrated, while the layer shown on figure a and b where the percentage of HBTP is 40 %, is more spread out and single fibre of HBTP are easily to see.

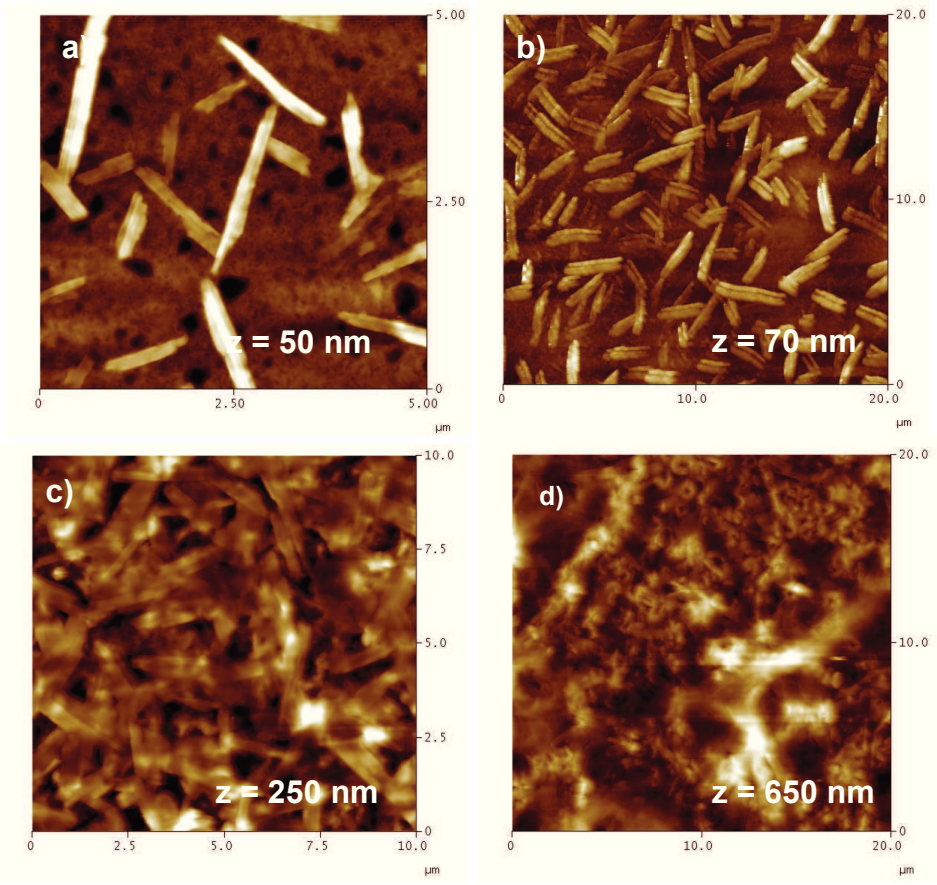

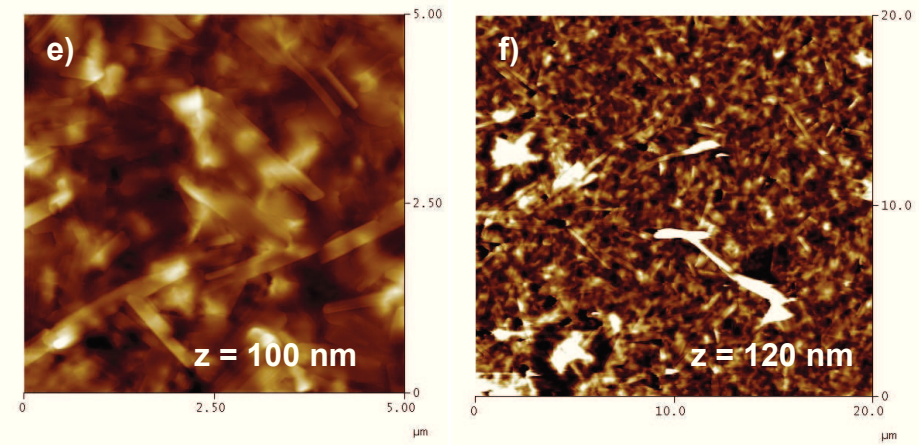

Figure 7.6.4.1. AFM images of HBTP/PCBM films on glass substrates for different ratio a, b) HBTP/PCBM=40%/60% filtered; c, d) HBTP/PCBM=50%/50% filtered; e, f) HBTP:PCBM=50%/50% non filtered.

7.6.5. Photoluminescence measurements

The photoluminescence (PL) measurements on the blend films with all ratios were carried out with a Time-Correlated Single Photon Counting system (TCSPC) and a pulsed laser diode (λ_{ex}=371nm, pulse width ~40 ps, maximum output ~5 mW). No PL was detected suggesting quenching from the PCBM.

7.7 Conclusion

- In summary, we present a novel, small-molecule donor system

HBTP, for use in organic plastic solar cells, with electron acceptor molecule PCBM.

- The best performance were reported for non filtered HBTP/PCBM device but even non filtered devices do not show enough good results to use HBTP for photovoltaic applications.

- HBTP dissolved poorly in chlorobenzene. Even at high temperature (~100 °C) the solution quality was still poor and it was possible to see small particles. Different solvents should be investigated.

- Annealing has fundamental influence of the performance of the device. It doubles both the J_{sc} and V_{oc}. The optimum annealing temperature was 100 °C for 5 min.

- A thicker active layer absorbs more light but is not homogeneous enough.

- The morphology of the film is not satisfactory due to the presence of isolated domains of HBTP. They helped electrons and holes to reach the electrodes but not the dissociation of excitons.

- Other type of electrodes (e.g. Al/Ca) or different type of the deposition (evaporation) should be investigated.

References

[1] B. Walker et al., *Adv. Funct. Mater*. **2009**, 19, 3063–3069.

[2] E. Bundgaard, F.C. Krebs, *Sol. Energy Mater. Sol. Cells* **2007**, 91, 954.

[3] C. J. Brabec et al, A*pplied Physics Letters,* **2002**, 80, 1288.

[4] G. Li et al, *Nature Materials,* **2005**, 4, 864.

[5] S.S. Sun, N. S. Sariciftci, *Organic Photovoltaics-Mechanisms, Materials& Devices*, **2005**, 129.

[6] R. Kroon et al, *Polym. Rev.* **2008***,* 48, 531.

[7] J. Roncali, *Accounts of Chem. Research,* **2009,** 42, 11, 1719-1730.

[8] M.T. Lloyd et al., *Materials Today*, **2007**, 10, 11.

[9] B. P. Rand et al, *Prog. Photovolt.*, **2007**, 15 659–76.

[10] S.Yoo et al, *Appl. Phys. Lett,* **2004**, 85 5427–9.

[11]M. Hiramoto et al, *Mol. Cryst. Liq. Cryst*, **2006**, 455, 267–75.

[12] K. Walzer et al, *Chem. Rev.*, **2007,** 107 1233–71.

[13] B. Johnev, K. Fostiropoulos, *Sol. Energy Mater. Sol. Cells,* **2008** 92 393–6.

[14] A. Colsmann et al, *Appl. Phys. Lett.,* **2006,** 89, 203506.

[15] W. Brutting et al, *Macromol. Symp.,* **2008,** 268 38–42.

[16] J. Xue et al, *Appl. Phys. Lett,* **2004**, 85, 5757–9.

[17] A. Opitz et al, *J. Appl. Phys.,* **2007**, 101, 063709.

[18] V. D. Mihailetchi et al, *Adv. Funct. Mater.,* **2006**, 16, 699–708.

[19] B. Domercq et al, *Mol. Cryst. Liq. Cryst.,* **2008,** 481 80–93.

[20] D. H. Kim et al., *Current Applied Physics,* **2010***,* 10, 985–989.

[21] S.E. Shaheen et al, *Appl. Phys. Lett.*, **2001**, 78, 841–3.

[22] G. Li et al, *J. Appl. Phys.,***2005**, 98, 043704

[23] M.W. Ma et al, *Adv. Funct. Mater.* **2005**, 15, 1617–1622.

[24] H. Hoppe, N. S. J. Sariciftci, *Mater. Chem.*, **2006**, 16, 45–61.

[25] X. Yang, et al., *Nano Lett.* **2005**, 5, 579–583.

[26] V. D. Mihailetchi et al, *Adv. Funct. Mater.*, **2005**, 15 795–801.

[27] Y. Peumans, J. Forrest, *Appl. Phys*., **2003,** 93, 7, 1.

[28] Y. Peumans, J. Forrest, *Letters of Nature*, **2003,** 425.

[29] J.A. Mikroyannidis et al, *Appl. Mater.& Interfaces*, **2010**, 2, 1, 270-278

[30] M.Gritan, M.Rusu, *Solar Energy Materials & Solar Cells*, **2010**, 446-450

8 Conclusion

In this thesis we have studied the mechanisms of the film structure formation of a PV applicable thin organic films, and how this impacts upon the photovoltaic efficiency of an OPV device.

To achieve this goal, Chapter 2 and 3 are an introduction to the state of the art on conjugated materials and PV applications. Important parameters of the process to control the morphology of the film have been identified as well as the physical issues of the problem, which suggest the optimal device structure.

Chapter 4 reports of experiments performed on P3HT and PCBM bulk heterojunction solar cells where different preparation conditions were applied. Different thermal annealing temperature, spin speed deposition of the photoactive layer, cooling rate and ultrasonicated treated blend were studied. Nanostructed morphology of the P3HT-PCBM was investigated and confirm with AFM analysis. Devices show

the best performance when the blend of the donor-acceptor material is treated with ultrasounds before the deposition, which result in more homogenous film, with annealing temperature at 140 °C for 10 min and slow cooling afterwards. In these conditions best results were: IPCE of 3.15% Jsc of 9.13 mA*cm^2, FF of 0.60 and Voc of 0.58.

We explained the high efficiency: as the ability of the blend of P3HT-PCBM to phase separate and crystallize into desirable BHJ morphologies after processing. This, in turn, allows efficient charge separation and transport. This was confirmed by AFM analysis where the formation of elongated PCBM nanocrystals providing efficient percolation paths for the electron where observed.

In Chapter 5 we reported on an investigation made on the effect of post-treatment production processes such as thermal annealing and external electric field application. The chapter focuses in finding an alternative to high temperature treatments for low-cost low-temperature fabrication of solar cell devices and finds a possibility in the use of an external electric field in absence of any post-thermal treatment.

In summary, the effect of annealing under external voltage on the PV characteristics of P3HT/PCBM encapsulated devices and influence of external voltage without thermal treatment were investigated. Results showed that an applied external electric field greater than the open-circuit voltage of the device injects additional charges into the polymer bulk and therefore may lead to a modified orientation of the polymer chains inside the photoactive layer along the direction of electric field. The ordered structure induced by the modified orientation of the polymer chains combined with the efficient percolation pathways increases the mobility of charge carriers. Moreover, our results showed that the effect of an applied electric field in isolation (without annealing treatment) is sufficient to obtain efficiencies given by the combined process (electric field and annealing) at the expense of higher applied voltage. However, this methods gives gains in terms of reduction of temperature and complexity of the fabrication process. In our opinion, this method can

easily be integrated into large area and low-temperature fabrication process for the future development of flexible polymer solar cells

Beside the study of the factors driving the efficiency of OPVs, stability over time is a major issue, too often not properly considered, if not at all. Organic solar cells are complicated multilayer structures where each component may fail for different reasons and layers may even interact chemically and physically in ways that may cause degradation. Fortunately, newer materials like P3HT are less prone to degradation (e.g., oxidation). Most organic solar cells today rely on the formation of bulk heterojunction. The phase-separation morphology, developed through the process of annealing is very important to obtain efficient devices. But this structure is not at the thermodynamic equilibrium, so further structural changes can occur, especially when devices are heated. More stable devices have already been made and progress in this research field is important for polymer solar cells to have a future as commercial devices. Fabrication in glove boxes followed by immediate encapsulation is a common laboratory technique used to maximize device lifetimes and improve stability. Unfortunately, large-scale production of OPVs in inert environments is not feasible. In order to keep down costs, ambient processing of organic solar cells is essential. New techniques need to be investigated to let organic solar cells compete with silicon technology and high customer request for efficient and long lifetime solar cells.

Finally, controlling the morphology of the device is only a part of the path to high-efficient OPVs. The choice of the material influences both electrical properties as the processes for the correct controlling of the morphology of the active layer of devices. Chapter 7 completes this thesis with the characterization (in photovoltaic terms) of a new small-molecule donor system, HBTP, for use in organic plastic solar cells, with electron acceptor molecule PCBM. With this material the best performance were reported for non filtered HBTP/PCBM device but even non filtered devices do not show enough good results to use HBTP for photovoltaic applications. As a matter of fact HBTP dissolved poorly in

chlorobenzene. Even at high temperature (~100 °C) the solution quality was still poor and it was possible to see small particles. Thus, for this material different solvents should be investigated. It was clear from the AFM images that the morphology of the film is not satisfactory due to the presence of isolated domains of HBTP. They help electrons and holes to reach the electrodes but do not support the dissociation of excitons.

To conclude, this thesis has investigated materials, production treatment, and post-production solutions for degradable organic thin films for photovoltaic applications. Controlling the morphology, together with new materials investigation, is the way to increase electrical performances of these devices. In this thesis we have focus on several aspects of the fabrication of solar cells and we have proposed an approach based on the application of an external electric field to be applied in low temperature fabrication processes.

Spin coated thin film and phase separation

A.1. Spin-coating

Spin-coating is a process used for fabricating thin polymer films from solution. It consists of dispensing a drop of the polymer solution onto a substrate. The substrate is held fixed onto a disc holder by means of vacuum, which is then rotated at a high speed (from hundreds up to several thousand revolutions per minute). The effect of the spinning motion is to spread out the solution on the substrate, forming a thin solid film [1]. The process can be broken down into the following four stages (see Figure A.1.1):

0. Deposition;
1. Acceleration;
2. Film thinning; and

3. Drying.

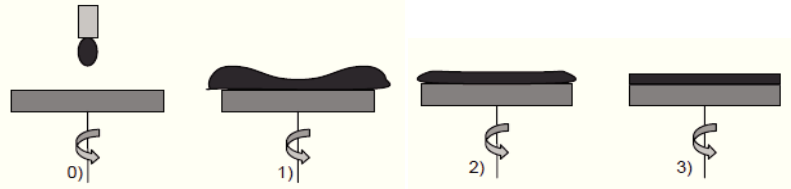

Figure A.1.1. The stages of spin-coating, 0) deposition of solution, 1) spreading during acceleration tofinal spin speed, 2) film thinning by outflow and evaporation, 3) drying by evaporation.

In the first phase, due to the rotation of the disc, only the ~10% of fluid remains on the substrate. After this stage the film is thin enough to co-rotate with the substrate. It has been reported that the dispensed volume of solution and the acceleration rate have little effect on the final thickness and uniformity of the film. However, it is recommended to keep the acceleration rates above ~10 seconds [2].

The second stage is characterized by viscous forces caused by the flow of the fluid off the substrate, and the evaporation of solvent. In this stage the final thickness and homogeneity of the film is determined.

However, when the viscosity of the film is high and, consequently, the flow is drastically reduced; stage 3 becomes the most important phase of the process. In this case solvent evaporation becomes the dominant mechanism [1].

A.2. Film formation and thickness

As described above, stage 2 of the spin coating process involves the main mechanism determining the final film thickness (h_f) [3], which is proportional to the spin speed (Ω) [1,3]:

$$h_f \propto \frac{1}{\sqrt{\Omega}}$$

The spin speed determines the radial flow and the evaporation rate. Higher values of the spin speed will result in a decrease of the film thickness [3]. However, viscous forces insist on the flow against the centrifugal force caused by the spin speed [4]. Therefore, the film thickness depends also on the viscosity of the solution, that in turn depends strongly on its concentration. The higher the concentration the higher the viscosity due to solvent evaporation during stage 2 of the spin-coating process. Thus, in order to obtain thin films an opportune initial concentration (or initial viscosity) must be chosen. High values will determine the film to reach earlier the point in which the radial flow ceases, and this will lead to a thicker film [1].

The evaporation of solvent can be modeled as a mass transfer process from the liquid film to the surrounding atmosphere, with rate of evaporation at the surface determined by: the vapour pressure of the solvent; the spin speed; and the conditions of the surrounding atmosphere (e.g. temperature, humidity). It is of great importance the correct choice of solvent.

For instance, a high vapour pressure solvent solution (such as chloroform) will result in a thicker but less phase separated blend film compared to a film spin-coated from lower vapour pressure solvents (such as xylene or chlorobenzene); if the spin-speed and concentration of the solution are the same in both cases.

Another aspect of the choice of solvent has to do with the relative solubility of the blend components in the used solvent. Walheim et al [5] showed that the topography of a spin-coated polymer blend film was affected as a result of a difference in solubility between the two blend polymers in the common solvent.

At the end of the second stage, when the radial flow ceases, the solvent becomes trapped inside the film and the evaporation rate will be limited by the diffusivity of the solvent molecules to the surface. With increasing polymer concentration the diffusivity decreases. The decrease in evaporation rate due to the decrease in diffusivity does not become significant until the third stage of the spin-coating process [4].

A.3. Phase separation in spin-coated thin films

Removal of solvent, when spin-coating homogeneous blends consisting of two solid components and a common solvent, will lead the system into a metastable or unstable region of the phase diagram. The process allows the solvent quench not to occur instantaneously, thus, giving to the system some time to phase separate. Ultimately, the phase separation stops when the viscosity of the film becomes high enough to limit the mobility of the polymer chains [6].

Spin speed and the initial concentration of the solution influence the time available for phase-separation. The higher the spin speed the higher the solvent evaporation rate. High spin speeds lead to a decreased film thickness, but give the system less time to phase separate.

A.4. Effect of the interfaces on the film formation

The phase separation of the blend components may be influenced by the free surface and the interface with the substrate. In particular, the free surface tends to attract the component with lower surface energy [7,8], while, the substrate influences the wetting behavior of the blend solution.

The mechanism is similar in both cases and both may leads to composition-gradients in the film.

As a result of random fluctuations in composition, a polymer blend at an unstable region of the phase diagram, generates compositional waves (spinodal waves). While in the bulk these waves are of random directions, in the presence of an interface the direction and phase of the spinodal waves may become fixed, propagating perpendicularly from the interface [9,10]. The results of several structure formation models [11-14] show that surface directed spinodal decomposition induces the formation of stratified phases in the early stage of spin-coating that can then either be frozen in [9,15,16] as a result of a rapid quench, or break up by interfacial instabilities to yield lateral domains [13,13,17].

A.5. Study of the morphology

To study the morphology of thin polymer blend films a variety of different experimental techniques and methods are available.

Techniques for imaging the surface topography of the blend thin films are:

- atomic force microscope (AFM), which is the most commonly used;
- Kelvin probe force microscopy (KFM) [18];
- scanning near field optical microscopy (SNOM) [19];
- scanning electron microscopy (SEM) [20];
- transmission electron microscopy (TEM) [21]; and
- scanning transmission x-ray microscopy (STXM) [22].

Chemical analysis of polymer blend composition at the film surface can be obtained by:

- photoelectron spectroscopy [12];
- Auger electron spectroscopy; and
- static secondary ion mass spectrometry (SIMS).

Structural properties of the blend films, e.g. crystallinity, can be studied by X-ray diffraction (XRD) [23].

For information on the vertical (in depth) morphology, nuclear reaction analysis (NRA) [24] or cross sections analysis with microscopy techniques, e.g. SEM, can be used.

Depth profiling of the chemical composition can be obtained by ion sputtering in combination with Auger electron spectroscopy [25] or by dynamic secondary ion mass spectrometry (SIMS) [26]. For example, dynamic SIMS has been used to analyze both the diffusion of aluminium and indium from the electrodes (Al and ITO) into the polymer film [26], and the spatial distribution of the blend components in the active layer [27].

References

[1] C.J. Lawrence, *Phys. Fluids* **1988,** *31*, 2786.

[2] W.W. Flack et al, *J. Appl. Phys.* **1984,** *56*, 1199.

[3] D. Meyerhofer, *J. Appl. Phys.* **1978,** *49*, 3993.

[4] D.E. Bornside et al, *J. Appl. Phys.* **1989,** *66*, 5158.

[5] S. Walheim et al, *Macromolecules* **1997,** *30*, 4995.

[6] A. Budkowski et al, e-Polymers, **2002**

[7] F. Garbassi et al, in *Polymer Surfaces: From physics to technology*, Wiley, Chichester, **1998**

[8] R.A.L. Jones et al, *Phys. Rev. Lett.* **1989,** *62*, 280.

[9] M. Geoghegan et al, *Polymer* **1994,** *35*, 2019.

[10] R.A.L. Jones et al, *Phys. Rev. Lett.* **1991,** *66*, 1326.

[11] M. Sprenger et al, *Interface Sci.* **2002,** *11*, 225.
[12] C. Ton-That et al, *Polymer* **2001,** *42*, 1121.
[13] S.Y. Heriot, R.A.L. Jones, *Nat. Mater.* **2005,** *4*, 782.
[14] A. Budkowski et al, *Macromolecules* **2003,** *36*, 4060.
[15] C. Ton-That et al, *Macromolecules* **2000,** *33*, 8453.
[16] A. Bernasik et al, *Synth. Met.* **2004,** *144*, 253.
[17] J. Raczkowska et al, *Macromolecules* **2004,** *37*, 7308
[18] H. Hoppe et al, *Nano Lett.* **2005,** *5*, 269.
[19] T. Kietzke et al, *Synth. Met.* **2005,** *152*, 101.
[20] C.M. Ramsdale et al, *Physica E* **2002,** *14*, 268.
[21] H. Hoppe et al, *Synthetic Metals* **20,** *152*, 117.
[22] C.R. McNeill et al, *Nano Lett.* **2006,** *6*, 1202.
[23] W. Ma et al, *Adv. Funct. Mater.* **2005,** *15*, 1617.
[24] A.M. Higgins et al, *J. Phys.: Condens. Matter* **2005,** *17*, 1319.
[25] M. Drees et al, *J. Appl. Phys.* **2005,** *97*, 036103.
[26] C.W.T. Bulle-Lieuwma et al, *Appl. Surf. Sci.* **2002,** *203-204*, 547.
[27] C.W.T. Bulle-Lieuwma et al, *Appl. Surf. Sci.* **2004,** *231-232*, 274

Atomic Force Microscopy

B.1. Atomic force microscopy

Atomic force microscopy (AFM) is a scanning probe technique developed for high-resolution surface topography measurements of insulators by Binnig and coworkers in 1986 [1]. It is based on the detection of interactions between a very sharp tip and the sample surface [2,3].

An AFM can be used in different modes:

- *contact mode*, where it detects the repulsive or attractive forces existing at close distance between the tip and the sample on the basis of the deflection cantilever-type spring with the tip attached in one end;
- *tapping mode*, where it probes the forces by oscillating the tip and cantilever above the surface and measure the damping of the vibration amplitude and the shift in resonance frequency;

- detection of *long range forces* and interactions, such as electrostatic or magnetic forces, by scanning special kinds of tips at a certain distance above the sample surface at which the influence of short-range forces is negligible.

B.2. Main instrument parts

The main components of an atomic force microscope consist of [3]:

- a piezoelectric ceramic scanner, which moves either the tip and/or the sample in x, y and z directions;
- the probe i.e. the tip and cantilever;
- a detector system, commonly a laser beam reflected on the back of the cantilever; and
- a position sensitive photodetector, which use the detector signal to adjust the vertical position or the oscillation of the tip (Figure A.2.1).

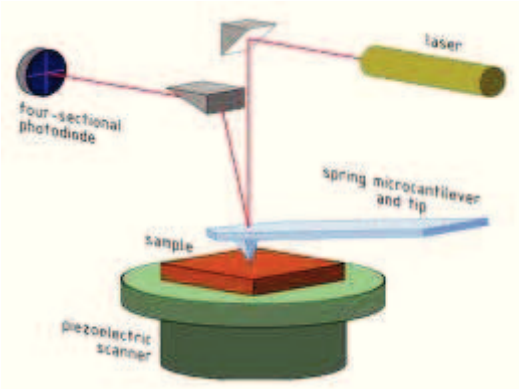

Figure A.2.1. Schematic images of the main components in AFM.

B.3. Tip-sample interactions

Van der Waals interactions dominate the potential energy of the interaction between two molecules (electrically neutral and non-magnetic) at a distance of one to tens of nm. They consist of three different components [2,4]:

- *polarization*, denoting the interaction between two molecules with permanent dipoles or multipoles;
- *induction*, which refers to induced dipoles from the interaction between one polar and one neutral molecule; and
- *dispersion*, which is the interaction between two non-polar molecules and is generally assumed to be the most significant.

The van der Waals potential gives rise to an attractive force between atoms and molecules. When atoms come too close their electronic charge distributions overlap, resulting in a Columbic repulsion force, which prevents the complete collapse of matter [5] and eventually becomes much larger than the attraction from the van der Waals potential (at short distances, i.e., a few Ångström).

In AFM measurements the probe is subjected to both the attractive and repulsive forces arising from the potential between the probe tip and the surface. Depending on which operating mode is used different forces or force gradients are probed:

- in contact mode the tip is placed within only a few Ångström of the sample surface and the repulsive forces are dominant. In this mode it is primarily the atomic short-range repulsive forces that are probed and a topographic image of the sample surface is obtained on basis of the cantilever deflection [4].
- in non-contact mode the tip is scanned above the surface probing the attractive van der Waals forces. In this mode, the amplitude of the oscillation of the tip at a particular frequency is kept constant, resulting in a height image. It is also possible to image the sample

surface based on the phase or frequency shift using a lock-in amplifier. By mapping the change of phase, an image of a variety of interaction forces is obtained, a so called phase image [2].

- at longer distance the attractive van der Waals force decays rapidly and instead long-range interactions, such as electrostatic attraction or repulsion, and magnetic interactions, become significant [2].
- In tapping mode the tip and cantilever are also oscillated but with a larger amplitude than for non-contact mode so that the tip comes in intermittent contact (tapping) with the sample surface. Similar to non-contact mode, the damping of the amplitude and/or the shift in phase can be used as the feedback signal resulting in height and phase images respectively. Tapping mode AFM is widely used for imaging the surface of polymer films. In polymer blends, phase-separated lateral domain structures may give rise to a contrast in the phase image [6].

B.4. Scanner

The most commonly used scanner is a hollow-tube scanner [2]. It consists of a tube of a piezoelectric material which is coated with a thin metal electrode on both the inner and outer surface [4]. The electrode on the outer surface is separated into four isolated segments. Vertical motion of the scanner is controlled by a voltage applied between the inner and outer electrodes. For lateral motion a voltage is applied over the oppositely located outer electrodes resulting in a bending of the tube. The choice of piezoelectric material and the dimensions of the tube determine the scan range of the scanner [2].

B.5. Force probes

The force probe consists of a sharp tip mounted on a cantilever. The cantilever act as a spring with a deflection following Hooke's law [4]

$$F = c\Delta z$$

where F is the force, c is the spring constant and Δz is the deflection. To obtain as large a deflection as possible for the small forces acting between the tip and the sample a soft cantilever, i.e. a small spring constant, is required. It is also necessary that the cantilever should have a high resonant frequency so to minimize the sensitivity to mechanical vibrations.

B.6. Detection

For detecting the deflection of the cantilever, a technique with sub-Ångström resolution is needed. It is also required that the detection technique should be easy to implement and have a negligible influence on the cantilever deflection itself. Nowadays, detection is commonly based on optical methods, and the most common is the laser beam deflection method [4]. This method uses a laser light that is reflected off the back of the cantilever and detected by a position sensitive detector, usually a four-segment photodiode. The vertical and lateral motions of the cantilever are determined by adding and subtracting (in different combinations) the signals from the four segments (quadrants) [2].

References

[1] G. Binnig et al, *Phys. Rev. Lett.* **1986,** *56*, 930.

[2] D. Bonnel (Ed.), *Scanning Probe Microscopy and Spectroscopy: theory, techniques, and applications*, Wiley-VCH, New York, **2001**,

[3] S.N. Maganov, M.-H. Whangbo, in *Surface Analysis with STM and AFM*, VCH, Weinheim, **1996**.

[4] R. Wiesendanger, in *Scanning Probe Microscopy and Spectroscopy. Methods and Applications.*, Cambridge University Press, **1994**.

[5] P.W. Atkins, in *Physical Chemistry*, Oxford University Press, Oxford, **1978**.

[6] P. Leclere et al, in *Advances in Scanning Probe Microscopy of Polymers*, (Eds: V.V. Tsukruk and N.D. Spencer), Wiley-VCH, Weinheim, **2000**, 117.

Materials

In this appendix a summary of characteristics of materials used in this thesis is given.

C.1. Poly(3-hexylthiophene-2,5-diyl) – P3HT

From Sigma Aldrich

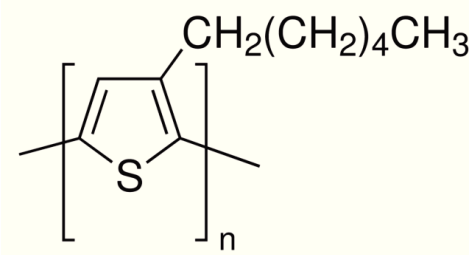

PROPERTIES	
Product number	445703
Formula	$(C_{10}H_{14}S)_n$
Regiregiularity	≥ 90 %
Molecular weight	
Fluorescence	λ_{ex} 443 nm; λ_{em} 568 nm in chloroform
Conductivity	~10^3 S/cm (when doped with Iodine)
Mp	238 °C
Orbital energy	3 eV

Greater than 90% head-to-tail regiospecific conformation. Good processibility, environmental stability and electroactivity.

2. [6,6]-Phenyl C_{61} butyric acid methyl ester - PCBM

From Sigma Aldrich

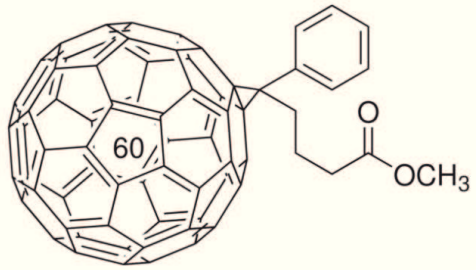

PROPERTIES	
Product number	684430
Formula	$C_{72}H_{14}0_2$
Formula weight	910.88 g/mol
Purity	≥ 99.0 %
Description	functionalized fullerene
Solubility	chlorobenzene: soluble organic solvents: soluble toluene: soluble
Orbital energy	6.1 eV

C.2. HBTP

See Chapter 7.1

C.3. Electrodes

C.3.1 Aluminum –Al

From Sigma Aldrich

PROPERTIES	
Product number	266558
Formula	Al
Formula weight	26.98 g/mol
Purity	99.999 %
Form	wire
Autoignition temp.	1400 °F
Resistivity	2.6548 μΩ-cm
Diam.	1.0 mm
Bp	2460 °C (lit.)
Mp	660.37 C (lit.)
Density	2.7 g/mL at 25 C (lit.)

C.3.2 Indium tin oxide – ITO

From Visiontek Systems

PROPERTIES	
Product number	
Formula	$In_2O_3 \cdot (SnO_2)_x$
Description	coated slide
Surface resistivity	~15 Ωhm/square
L × W × thickness	14mm × 14 mm × 1.1 mm
transmittance	~89% (nominal at 550 nm)
Refactive index	n20/D 1.517
Thickness of ITO coating	150 nm

C.4. Solvents

4.1 Chlorobenzene – C_6H_5Cl

From Sigma Aldrich

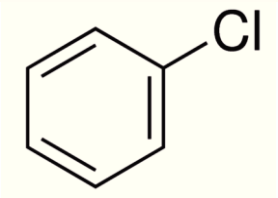

PROPERTIES	
Product number	270644
Formula	C_6H_5Cl
Formula weight	112.56 g/mol
grade	CHROMASOLV®
	for HPLC
vapor density	3.86 (vs air)
vapor pressure	11.8 mmHg (25 °C)
assay	99.9%
autoignition temp.	1178 °F
purified by	glass distillation
expl. lim.	7.1 %
total impurities	≤0.01% water
evapn. residue	<0.0003%
refractive index	*n*20/D 1.524(lit.)
bp	132 °C(lit.)
mp	−45 °C(lit.)
density	1.106 g/mL at 25 °C(lit.)
λ	H_2O reference
UV absorption	λ: 288 nm A_{max}: 1.0
	λ: 290 nm A_{max}: 0.40
	λ: 300 nm A_{max}: 0.05

	λ: 325 nm A_{max}: 0.04
	λ: 360-400 nm A_{max}: 0.01

4.2 2-propanol – C_3H_8O

From Sigma Aldrich

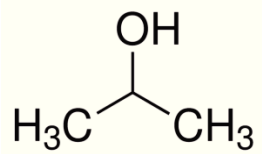

PROPERTIES	
Product number	34863
Formula	C3H8O
Formula weight	60.10 g/mol
grade	CHROMASOLV®
	for HPLC
vapor density	2.1 (vs air)
vapor pressure	33 mmHg (20 °C)
	44 mmHg (25 °C)
assay	99.9%
autoignition temp.	750 °F

expl. lim.	2 %
total impurities	≤0.0005% non-volatile matter
	≤0.001% free acid (as C_2H_5COOH)
	≤0.05% water (Karl Fischer)
color	APHA: ≤10
transmittance	210 nm, ≥20%
	220 nm, ≥50%
	230 nm, ≥75%
	260 nm, ≥98%
refractive index	*n*20/D 1.377(lit.)
bp	82 °C(lit.)
mp	−89.5 °C(lit.)
density	0.785 g/mL at 25 °C(lit.)
UV absorption	λ: 205 nm A_{max}: ≤1.0
	λ: 210 nm A_{max}: ≤0.70
	λ: 220 nm A_{max}: ≤0.20
	λ: 230 nm A_{max}: ≤0.10
	λ: 260 nm A_{max}: ≤0.01
	λ: 400 nm A_{max}: ≤0.01

4.3. Acetone - C_2H_6O

From Sigma Aldrich

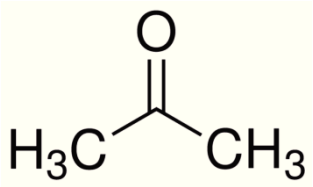

PROPERTIES	
Product number	270644
Formula	C_2H_6O
Formula weight	58.08 g/mol
grade	CHROMASOLV®
	for HPLC
vapor density	2 (vs air)
vapor pressure	184 mmHg (20 °C)
assay	≥99.8%
expl. lim.	13.2 %
total impurities	≤0.0005% non-volatile matter
	≤0.002% free acid (as CH_3COOH)
	≤0.1% water (Karl Fischer)
transmittance	330 nm, ≥15%

	335 nm, ≥50%
	340 nm, ≥80%
	350 nm, ≥98%
refractive index	*n*20/D 1.359(lit.)
bp	56 °C/760 mmHg(lit.)
mp	−94 °C(lit.)
density	0.791 g/mL at 25 °C(lit.)

C.5. Epoxy

A light-curable epoxy which sets at wavelengths of up to 600 nm and is safe for use with most organic materials Ossila's EE1 Encapsulation epoxy can be used as an adhesive for organic light-emitting diodes and organic photovoltaics without damaging the polymer or cathode. In conjunction with a glass coverslip it can provide a robust barrier against ingress of oxygen and water to provide extended lifetimes for measurement and storage. Curing can be achieved with UV or visible wavelengths as long as 600 nm and at high intensities (100mW/cm^2) takes as little as 5 seconds. At lower intensities such as those found in many lab-scale light boxes curing time may be considerably longer at up to 20 minutes.

PROPERTIES	
Viscosity	~300 cps@23C
Colour	Amber to light brown transparent liquid

Cure Schedule	5 to 30 seconds at 250 to 600 nm at 10 - 100mW/cm^2
Refractive Index	1.4957
Specific Gravity	1.17
Cured Shore D Hardness	92+ D
Tensile Strength	~7,000 psi
Elongation	< 2%
Glass Transition Temperature	130C
CTE	20x10^{-6}
Shelf Life	12 months at 23C
Dielectric constant	3.94@60Hz@20C
Volume resistivity	3.0x10^14Ohm cm

References

[1] http://www.sigmaaldrich.com/

[2] http://www.visionteksystems.co.uk/

[3] http://www.ossila.com/